# "HYPERSONIC VISCOUS SLIP FLOW PAST NON-INSULATED WEDGES"

By
V. K. MATHEWS



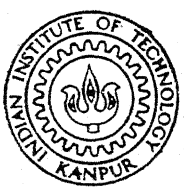


DEPARTMENT OF AERONAUTICAL ENGINEERING
**INDIAN INSTITUTE OF TECHNOLOGY, KANPUR**

DECEMBER-1978

# "HYPERSONIC VISCOUS SLIP FLOW PAST NON-INSULATED WEDGES"

A Thesis Submitted
in Partial Fulfilment of the Requirements
for the Degree of
MASTER OF TECHNOLOGY

By
V. K. MATHEWS

to the
DEPARTMENT OF AERONAUTICAL ENGINEERING
**INDIAN INSTITUTE OF TECHNOLOGY, KANPUR**
DECEMBER-1978

## CERTIFICATE

This is to certify that the thesis entitled "Hypersonic Viscous Slip Flow Past Non-Insulated Wedges" by Mr. V.K. Mathews is a record of work carried out under our supervision and has not been submitted anywhere else for a degree.

(A.C. Jain)
Professor,
Department of Aeronautical Engineering,
I.I.T. Kanpur.

(R.N.Gupta)
Professor,
Department of Aeronautical Engineering,
I.I.T. Kanpur.

Dated : December 30, 1978.

*With Love Affection and Respect to*

*My*

*Ammachi and Appachan.*

*ABSTRACT*

*An approximate integral technique has been developed for the hypersonic strong interaction flow over two-dimensional slender bodies with slip and temperature-jump effects. With the help of this approximate method, results have been obtained to understand the effects of slip and temperature jump on the various characteristics of flow such as heat transfer, skin friction, surface pressure distribution and boundary layer growth. The flow governing momentum and energy integral equations are solved by using a linear velocity profile and a second degree enthalpy profile, the induced pressure being described by the full tangent-wedge approximation. For both slip and no-slip cases, analytical solutions are developed for the strong - interaction region by using the leading term of the tangent-wedge approximation. This is used to obtain the initial conditions for the numerical integration of the momentum and energy equations employing the full tangent-wedge approximation. The present results cover a wide range of flow situations with wall enthalpy ratios varying from 0.065 to 1, semi-wedge angle varying from 0° to 5°, Prandtl number varying from 0.75 to 1, and Mach number in the range of 10 to 20 for both slip and no-slip cases. Reasonable agreement is observed between the present results and the experimental as well as theoretical predictions of other investigators. It is observed from the*

*present computations that except for the extreme cold wall case, slip and temperature-jump at the surface are very important in predicting the hypersonic strong interaction flow close to the leading edge and in obtaining the physically plausible results. These results, further, help in bridging the gap between the experimental observations and theoretical predictions.*

*ACKNOWLEDGEMENTS*

*The author wishes to express his deep sense of gratitude to Professor A.C. Jain for his guidance and encouragement throughout the course of this work.*

*Nor would this work exist in its fullness without the all hearted helps of Professor R.N. Gupta. The author acknowledges immense debt to him.*

*Mr. Partho Chaudhury and Mr. S.R. Prasad are thanked for many stimulating discussions on the subject.*

*The author owes great debt to his friend Mr. P.V. Ramachandran for his help in the compilation of the thesis.*

*In an intangible, yet real way the author is indebted to his friends, to Messrs. K.P. Abraham, N. Mony, James Thomas, Dr. K.M. Varier and several others unnamed for their earnest helps and cooperation throughout the course of his M.Tech. programme.*

*Finally but by no means least, thanks to Mr.G.L.Misra for the excellent typing of the manuscript.*

*Mathews*

## Nomenclature

| | |
|---|---|
| $A$ | $H_b/H_\infty$ |
| $A_0$, $A_1$, $A_2$ | Functions used in the series solution for no slip case as defined in (3.16). |
| $a$ | Velocity of sound. |
| $a_0$, $a_1$, $a_2$, $\vdots$, $a_n$ | Coefficients in the series expansion for $\eta$ in (3.1). |
| $B$ | $\frac{1}{H_\infty}\left(\frac{\partial H}{\partial y}\right)_w$ |
| $B_0$, $B_1$, $B_2$ | Functions used in the series solution for no slip case as defined in (3.16). |
| $b$ | $\frac{\gamma+1}{4}$ . |
| $b_0$, $b_1$, $b_2$, $\vdots$, $b_n$ | Coefficients in the series expansion for $\psi$ in (3.1). |
| $c$ | $\frac{\mu_w}{\mu_\infty} \cdot \frac{T_\infty}{T_w}$ , Chapman Rubesin constant. |
| $C_1$ | a constant, $\sqrt{\pi/2}$. |

$C_2$ $\quad \frac{2\gamma}{\gamma+1} \times \frac{1}{Pr} \times \frac{2-\alpha}{\alpha}$ .

$C_f$ $\quad \frac{\tau}{1/2\ \rho_\infty\ u_\infty^2}$ , the skin friction coefficient.

$C_p$ $\quad$ Specific heat at constant pressure.

$C_v$ $\quad$ Specific heat at constant volume.

$e_1$, $e_2$ $\quad$ Slip parameters defined by equation (2.31).

$e_{11}$, $e_{22}$ $\quad$ Slip parameters for the leading edge defined by equation (2.25).

$f$, $g$ $\quad$ functions defined by equation (3.9).

$H$ $\quad$ Total enthalpy

$\bar{H}$ $\quad$ $H/H_\infty$.

$h$ $\quad$ A function defined by equation (3.9).

$K$ $\quad$ Thermal conductivity.

$k$ $\quad$ $M_\infty\ (\beta + \frac{d\delta}{dx})$

$k_1$, $k_2$ $\quad$ Two constants in the velocity profile.

$L$ $\quad \frac{\mu_w}{\rho_\infty\ u_\infty}$ , a characteristic length.

$\ell$ $\quad$ Length of the wedge or flat plate.

$m$, $n$ $\quad$ As defined by equation (2.37).

$P$ $\quad$ Pressure.

$\bar{P}$ $\quad$ $P/P_\infty$.

| | |
|---|---|
| Pr | Prandtl Number, $\frac{\mu C_p}{k}$ . |
| p, q | Index of expansion for $\psi$ and $\eta$ in (3.1). |
| $\dot{q}$ | heat transfer defined by (A.12). |
| R | Specific gas constant. |
| $Re_\ell$ | Reynolds number evaluated at the end of wedge $\frac{\rho_\infty u_\infty \ell}{\mu_\infty}$ . |
| $Re_x$ | Local Reynolds number $\frac{\rho_\infty u_\infty x}{\mu_\infty}$ . |
| r, s | Functions defined by equation (3.9). |
| St | Stanton number defined by equation (A.13). |
| T | Temperature |
| $\bar{T}$ | $T/T_\infty$. |
| u | Velocity component in x direction. |
| $\bar{u}$ | $u/u_\infty$. |
| $\bar{V}$ | Rarefaction parameter, $M_\infty \sqrt{c/Re_x}$. |
| v | Velocity component in y direction. |
| x | Distances along the wedge surface. |
| $\bar{x}$ | $x/\ell$ . |
| y | Distance normal to the wedge surface. |
| $\bar{y}$ | $y/\ell$ . |
| $\alpha$ | Energy accomodation coefficient. |
| $\alpha_1$, $\alpha_2$, $\alpha_3$, $\alpha_4$ | Functions as defined by equation (3.8). |

| | |
|---|---|
| $\beta$ | Semiwedge angle. |
| $\gamma$ | Ratio of specific heats, $C_p/C_v$. |
| $\delta$ | Boundary layer thickness. |
| $\zeta$ | Non-dimensionalised longitudinal distance, $\frac{x}{L}$. |
| $\eta$ | Non-dimensionalised boundary layer thickness, $\frac{\delta}{L}$. |
| $\lambda$ | Mean free path of molecules. |
| $\mu$ | Coefficient of viscosity |
| $\rho$ | density. |
| $\bar{\rho}$ | $\rho/\rho_\infty$. |
| $\sigma$ | Index of expansion for $\eta$ in (3.1). |
| $\tau$ | Viscous shear stress. |
| $\phi$ | y/L. |
| $\bar{\chi}$ | Strong interaction parameter, $M_\infty^3 (c/Re_x)^{1/2}$. |
| $\psi$ | BL, the non-dimensionalised enthalpy gradient. |
| $\omega$ | $M_\infty^2/\bar{P}$. |

Subscripts

| | |
|---|---|
| $\infty$ | Free stream conditions. |
| b | Properties of gas next to the wall. |
| e | quantities at the edge of boundary layer. |
| $\ell$ | Values based on wedge length. |
| w | quantities evaluated at the wall. |
| o | Free stream stagnation conditions. |

Superscripts

| | |
|---|---|
| i | Step-counter for integration. |
| j | Iteration counter. |

# TABLE OF CONTENTS


| | | | |
|---|---|---|---|
| ABSTRACT | | | i |
| ACKNOWLEDGEMENT | | | iii |
| NOMENCLATURE | | | iv |
| TABLE OF CONTENTS | | | viii |
| LIST OF FIGURES | | | ix |
| CHAPTER I | | INTRODUCTION | 1 |
| | §1.1. | Statement of the Problem. | 1 |
| | §1.2. | Review of Literature. | 3 |
| | §1.3. | Description of the Present Work. | 9 |
| CHAPTER II | | FORMULATION OF THE PROBLEM | |
| | §2.1. | Governing Equations. | 12 |
| | §2.2 | Boundary Conditions. | 13 |
| | §2.3 | The Integral Equations. | 15 |
| | §2.4. | The Velocity and Enthalpy Profiles. | 15 |
| | §2.5. | The Momentum Equation - A Working Form. | 17 |
| | §2.6. | The Energy Equation - A Working Form. | 24 |
| | §2.7 | Working Equations for No-slip Case. | 28 |
| CHAPTER III | | METHOD OF SOLUTION | |
| | §3.1. | Analytical Solution For Slip-Case. | 30 |
| | §3.2. | Analytical Solution For No-Slip Case. | 35 |
| | §3.3. | Numerical Integration Scheme | 37 |
| CHAPTER IV | | RESULTS AND DISCUSSIONS | 40 |
| | | CONCLUSION | 46 |
| BIBLIOGRAPHY | | | 48 |
| FIGURES | | | |
| APPENDIX | | | A1 |

## LIST OF FIGURES


Fig. 1. Flow Regimes Of The Hypersonic Rarefied Flow Past a Sharp Nosed Slender Body.

Fig. 2. Effect of Semiwedge Angle And Mach Number On Boundary Layer Thickness Distribution Over a Cold Wall.

Fig. 3. Effect of Wall Enthalpy Ratio On Boundary Layer Thickness Distribution Over a Flat Plate.

Fig. 4. Pressure Distribution As a Function of Rarefaction Parameter.

Fig. 5. Comparison Of Pressure Distribution Over a Flat Plate And Wedge.(Cold-Wall Case).

Fig. 6. Variation Of Skinfriction As a Function Of Rarefaction Parameter.(Effect Of Wall-Enthalpy Ratios On Skinfriction).

Fig. 7. Variation Of Skinfriction With Rarefaction Parameter.(Effect Of Semiwedge Angle On Skinfriction).

Fig. 8. Variation Of Stanton Number as a Function Of Rarefaction Parameter.(Effect Of Wall-Enthalpy Ratios On Stanton Number).

Fig. 9. Variation Of Stanton Number With Rarefaction Parameter. (Effect Of Semiwedge Angle, Mach Number And Prandtl Number On Stanton Number).

Fig. 10. Variation Of Slip Velocity With Rarefaction Parameter. (Effect of Wall-Enthalpy Ratios On Slip Velocity).

Fig. 11. Variation Of Slip Velocity As a Function Of Rarefaction Parameter. (Effect Of Semiwedge Angle And Mach Number On Slip Velocity).

Fig. 12. Variation Of Enthalpy-Jump With Rarefaction Parameter.

Fig. 13. Variation Of Temperature-Jump As a Function Of Strong Interaction Parameter.

Fig. 14. Variation Of Enthalpy Profiles With Distance Along The Wedge.

Fig. 15. Variation Of Enthalpy Across The Boundary Layer. (Effect Of Wall-Enthalpy Ratios On Enthalpy Distribution).

Fig. 16. Velocity Profiles At Various Stations Along The Surface. (Adiabatic Wall, Medium-Cold Wall And Extremely-Cold Wall).

# CHAPTER - 1

# INTRODUCTION

## §1.1. STATEMENT OF THE PROBLEM

The problem of hypersonic rarefied flow past slender bodies has been the subject of extensive theoretical as well as practical investigations for quite a long time. In addition to its practical importance in the simulation of flight of the hypersonic vehicles in a rarefied atmosphere, such a flow model embodies a wide spectrum of flow regimes in gas dynamics from the kinetic flow close to the leading edge to the conventional continuum flow towards the downstream portions of the vehicle. Since the flow undergoes several transitions from leading tip to downstream, one will have to resort to different analytical methods to deal with each regime.

At hypersonic speeds, the so called shockwave boundary layer interaction occurs when the rapid growth of boundary-layer displacement thickness near the leading edge displaces the external flow considerably. This phenomenon is the result of the low density of air due to the extremely high temperatures in the boundary layer at high Mach numbers. The displacement of the external flow gives rise to an induced pressure and imposes a negative pressure gradient on the boundary layer. Simultaneously the shockwave emanating from the leading edge

must increase in strength to account for the added flow deflection, so that the stream lines crossing it carry increased values of vorticity and entropy. On blunt bodies the pressure induced by viscous interaction is generally insignificant in comparison to the bluntness-induced effects namely, the vorticity interaction. However, on sharp nosed slender bodies the viscous induced pressures may amount to several times the inviscid pressure. Also at hypersonic speeds the fluid density within the compressible boundary layer is relatively low which gives rise to the possibility of slip flow over the surface.

A pictorial representation of the flow-field being discussed is given in Fig. 1, with the various regimes delineated. In both strong and weak interaction regions the surface pressures are found to be linearly dependent on the strong-interaction parameter $\bar{\chi}$ defined as $M_\infty^3 (C/Re_x)^{1/2}$. But as one moves further upstream the shockwave and boundary layer merge into each other and the pressure curve shows a "plateau" although the slope of the shockwave continues to increase towards the leading edge. This levelling off of the pressure and of parameters like skin friction, heat transfer etc. are attributed to the shockwave getting thickened and weakened towards the leading edge. Theoretical investigations of the recent past could give explanations to these experimentally noticed plateaus when slip and temperature-jump at the surface are accounted for. The various diversified regimes up to and

including the merged layer regime occuring in the flow model have been treated by the continuum approach, the flow being governed by the Navier-Stokes equations with the inclusion of velocity slip and temperature-jump boundary conditions at the body surface. Of course, in the region ahead of the merged layer regime the flow is highly rarefied and requires a kinetic theory treatment.

## §1.2. REVIEW OF LITERATURE

Though the interest in the problem of hypersonic flow past slender bodies had been with the researchers since a long time , it was only in 1952 that a real contribution to the field occured when Shen [ 1 ] attempted an analytical estimate of the viscous effects of hypersonic flow over an insulated wedge. Shen [ 2 ] suggested that the compressible boundary layer equations are valid in the viscous layer on the body as a first approximation and he was able to treat the shockwave boundary layer interaction problem with the help of a momentum integral method. Lees [ 3 ] solved the hypersonic strong interaction problem by using the Prandtl's boundary layer equations. He found that as Mach number increases the interaction region spreads downstream over the plate and the skin friction coefficient increases rapidly over its conventional value. However Lees disagrees with Shen's [ 2 ] argument that the static pressure variation across the boundary layer is of the order $(1/M_\infty^2)$, for Shen puts up this argument on the basis of the postulation that, $\rho \sim \frac{1}{T} \sim \frac{1}{M_\infty^2}$ , inspite of

the fact that T is certainly not of the order of $M_\infty^2$ near the outer edge of the viscous layer or near the surfaces for the case of heat transfer. Stewartson [4] extended Lees' [3] theory with a more complete discussion of the inviscid flow between the shockwave and boundary layer. He proposed the existence of a similar solution in the inviscid zone which may be joined to the similar solution in the boundary layer. He employed the von Kármán-Pohlhausen integral method and showed that the tangent-wedge approximation for the pressure on the plate used by Lees [3] is in deficit by ten percent.

Pai and Shen [5] extended Li and Nagamatsu's [6] non-adiabatic flat plate problem to wedges by using a generalized von Kármán-Pohlhausen integral method. In their analysis they used a temperature function 'S' to relate the absolute temperature and velocity. Where,

$$S = 1 - \frac{C_p T + \frac{1}{2} u^2}{C_p T_\infty + \frac{1}{2} u_\infty^2} .$$

The major assumptions underlying their analysis were

i) $Pr = 1$

ii) $\mu \sim T^n$.

Their results especially, those on surface pressure distribution were well supported by the similar solutions of Li and Nagamatsu [6]. Bertram [7] extended Kendall's [8] experimental investigations of hypersonic flow past flat plates

to thin wings with square and delta planforms. He found a greater value of the skin-friction coefficient which can not be explained by the conventional laminar boundary layer theory. Betram attributed this difference in skin-friction to the large values of induced pressures at hypersonic speeds.

In the light of experimental investigations in a low density wind tunnel Schaaf [9] suggested the existence of slip at the leading edge. In fact he was motivated by Lees [10] who in one of his very substantial papers established the linear variation of surface pressure with the strong interaction parameter. According to this result pressure must be infinite at the leading edge which is not expected to take place as the boundary layer assumptions are not valid in this region. Schaaf tried to modify Lees' theory so that the singularity in his formulation may be erased out. With the provision that the gas does not slip along the surface, such a modification would result in a surface pressure which is expected behind a normal shock. Therefore he concluded that the gas would have to slip along the surface invariably as the observed pressures were much less than what would have been behind a normal shock.

Though quite a few experimental [11], [12], [13] etc., as well as theoretical investigations [14], [15] etc., of the hypersonic slip effects have been made by many investigators, it was Talbot [16] who first suggested the criterion for slip near the leading edge. Talbot concluded that the

parameter $M_\infty(c/Re_x)^{1/2} = \bar{V}$ is appropriate for correlating the emergence of slip flow effects near the leading edge of a flat plate in hypersonic flow. He found that for $\bar{V} = 0.1$ or above slip would be a dominant phenomenon. Talbot interpreted the rarefaction parameter in two ways.

i) A measure of the ratio of the mean free path behind the shockwave to boundary layer displacement thickness.

ii) A measure of the ratio of the leading edge shockwave thickness to distance downstream from leading edge.

Laurmann [17] attempted a solution to the hypersonic slip flow problem over a flat plate by linearizing the Oseen's equations, with an idea of getting some valuable approximations to an otherwise intractable problem as well as serving as a guide to methods of treating the full non-linear equations. His solutions showed that in the hypersonic limit the effect of slip and temperature-jump are quite radical, resulting in a flow at the leading edge which was unperturbed from free stream state. In otherwords there exists perfect slip at the leading edge. Aroesty [18] with the help of a series solution argues that the slip effects alone are not adequate to explain the appearence of heat transfer plateau observed near the leading edge of a sharp flat plate in hypersonic flow as mentioned by Talbot. However, he agrees that the induced pressure and skin friction will exhibit a first order slip effect. Rudman and Rubin [19] developed a mathematical flow model incorporating

the effect of temperature-jump and slip at the surface. Their equations were valid throughout the boundary layer shock wave structure and inviscid core for flat plates and wedges, for a wide range of Mach numbers $\geq 2$. On the basis of the finite difference solutions, they put up the following conclusions.

i) Slip boundary conditions are necessary for $\bar{V} \geq 0.1$.

ii) Across the merged layer large gradients of pressure and density exists, the maximum density being on the surface.

iii) The merged layer passes asymptotically into the strong interaction flow.

Among the numerous experimental investigations, those performed by Vidal and Bartz [20] are considered to be quite reliable and elaborate and therefore have been quoted in the literature extensively. They carried out a detailed study of the hypersonic low density flow over flat plates and wedges in a hypersonic shock tunnel at Mach numbers of 18 to 24 and Reynold's numbers which produced conditions largely to span the transition between continuum flow to near free molecular flow, giving emphasis to determine the extend of slip and energy jump at the surface. His findings indicated that the then available theories substantially under-estimated the magnitude of slip velocity and energy jump. They discussed the viscous layer from a continuum view point and the first collision regimes from a kinetic view point. This model is an improved version of their own previous innovation [21]. Their results are in good agreement with those of Shorenstein and Probstein [22]

and Cheng [13] for pressure and shock wave shape, but heat transfer and skin friction are about 30 per cent larger than Cheng's. This error appears to stem from the approximation which Cheng has taken, namely, in the limiting case of $\gamma$ approaching unity

$$p/p_\infty \simeq M_\infty^2 \sin^2 \theta,$$

where $\theta$ is the shock angle.

In the vicinity of the leading edge, Vidal and Bartz found that free molecular limit is approached asymptotically with the first collision effects influencing the process.

Later, Kumar and Jain [24] developed an approximate integral method for the hypersonic flow past insulated wedges incorporating the effect of slip velocity at the surface. The pressure along the edge of the boundary layer is prescribed by the leading term of the full tangent-wedge approximation and the von Kármán-Pohlhausen method is used with a linear profile for the tangential component of velocity in the boundary layer. Chaudhury [25] extended this work with full tangent-wedge approximation so that the solutions are valid from strong-interaction to weak-interaction zones. He solved the insulated wedge problem by feeding the attenuated values of pressure outside the boundary layer from the approximate solution. More recently Menon [26] analysed the strong interaction problem incorporating the effects of slip and temperature-jump by a finite-difference technique suggested by Smith and Clutter.

Menon used an iterative procedure to obtain solutions to the slip flow problem from the no-slip series solutions of Chattopadhyay [27].

## §1.3. DESCRIPTION OF THE PRESENT METHOD

In the present analysis an approximate integral method is developed for the hypersonic viscous slip flow over wedges, which is relatively simpler from computational point of view and gives reasonably accurate results. We envisage an infinitesimally thin shockwave emanating from the leading edge and continuum hypothesis is assumed to be applicable to the flow field of interest namely the strong interaction regime, transition regime and weak interaction regime. The results have been obtained by integrating the boundary layer equations (2.1), (2.2) and (2.3), using slip and temperature jump boundary conditions on the surface.

Using the continuity equation a first integral of the momentum equation and energy equation is derived by assuming $u_e \simeq u_\infty$ and $H_e \simeq H_\infty$. Next, appropriate velocity and enthalpy profiles are to be chosen. The selection of the velocity and enthalpy profiles in any integral method is governed by the considerations of simplicity in the analysis on one hand and the possibility of satisfying more boundary conditions and compatibility on the other. A linear tangential velocity profile and a second degree enthalpy profile is found to be suitable for our purpose. The viscous-inviscid interaction is

represented by the full tangent-wedge approximation so that the solutions are valid from the fore-regions of the body to downstream stations. The system of non-linear partial differe-ntial equations (2.1), (2.2) and (2.3),is thus reduced to two second order ordinary differential equation (2.34) and (2.43), which are coupled and solved by the scheme discussed in Chapter III for the unknowns $\eta$ , the boundary layer thickness and $\psi$ , the enthalpy gradient at the wall. For no-slip case both these equations show singularity at the leading edge (i.e. at $x = 0$), hence the integration is started from a point slightly downstream. However, for slip case the integration is started right from the leading edge. For both slip and no-slip cases analytical solutions are provided for the leading edge region by a series solution procedure employing the leading term of the full tangent-wedge approximation. This also provides the initial conditions for the numerical integration of the original problem employing the full tangent-wedge approximation. Integration is carried down to weak interaction region far downstream from the leading edge.

Quite a wide range of flow situations have been considered with wall enthalpy ratios varying from 0 to 1, semi-wedge angles from $0^{\circ}$ to $5^{\circ}$, Mach numbers from 10 to 20 and Prandtl number from 0.75 to 1 for both slip and no-slip cases. A detailed comparison of the present results with the available experimental data and results of other theoretical investigations have been carried out. For cold wall cases present results are

compared with the experimental findings of Vidal and Bartz [20], Vidal and Wittliff [28] and Vas and McDougall [29] and a reasonable agreement is observed. Present results agree well with the locally similar solutions of Shorenstein and Probstein [22] and Cheng [13] and the finite difference results of Rudman and Rubins [19]. For insulated wedges a comparison is made with the approximate integral method of Kumar and Jain [24] and for no-slip case present results agree well with Chattopadhyay's [27] results. Another comparison is made with the recent results of Menon [26] who solved the problem by iterative finite-difference technique. These comparisons show the effectiveness and accuracy of the approximate method. Similar to the earlier investigations, the present analysis also shows that slip plays an important role in explaining the experimentally observed 'Plateaus' of constant pressure, heat transfer, skin friction etc. towards the leading edge and bringing the result closer to the experimental data.

# CHAPTER II

## FORMULATION OF THE PROBLEM

### § 2.1 GOVERNING EQUATIONS :

The governing equations for a steady, two dimensional, compressible flow are the following :

Continuity

$$\frac{\partial}{\partial x}(\rho u) + \frac{\partial}{\partial y}(\rho v) = 0 \tag{2.1}$$

Momentum

$$\left.\begin{aligned} \rho u \frac{\partial u}{\partial x} + \rho v \frac{\partial u}{\partial x} &= -\frac{dP}{dx} + \frac{\partial}{\partial y}\left(\mu \frac{\partial u}{\partial y}\right) \\ \frac{dP}{dy} &= 0 \end{aligned}\right] \tag{2.2}$$

Energy

$$\rho u \frac{\partial H}{\partial x} + \rho v \frac{\partial H}{\partial y} = \frac{\partial}{\partial y}\left[\frac{\mu}{Pr}\frac{\partial H}{\partial y} + \left(1 - \frac{1}{Pr}\right)\mu \frac{\partial}{\partial y}\left(\frac{1}{2}u^2\right)\right] \tag{2.3}$$

where $H = C_p T + \frac{1}{2}u^2$ (2.3a)

Equation of State

$$P = \rho R T \tag{2.4}$$

Also the viscosity-temperature relation $\mu = \mu(T)$, for the present investigation is assumed to be linear. Accordingly, the following relation has been utilized :

$$\frac{\mu_w}{\mu_\infty} = c\,\frac{T_w}{T_\infty}$$

where c is the Chapman-Rubesin constant.

## §2.2 BOUNDARY CONDITIONS

(a) Boundary conditions for the momentum equation :

At the surface of the wedge, for a no-slip flow situation, both the tangential and the normal components of velocity must be zero. However, for the strong-interaction region next to the merged-layer regime, the effects of slip will be important to account for. Accordingly, the boundary conditions have been given for slip and no-slip cases simultaneously.

i) At the surface of the wedge, i.e. at $y = 0$ :

$$\left.\begin{aligned} & u = v = 0, \quad \text{for no-slip case,} \\ \text{and} \quad & \\ & u = u_b = C_1 \lambda_w \left(\frac{\partial u}{\partial y}\right)_w \\ & v = 0 \qquad\quad \text{, for slip case} \end{aligned}\right\} \tag{2.6a}$$

where

$$C_1 = \sqrt{\frac{\pi}{2}} ,$$

$\lambda_w$ is the mean free path of the molecules at wall temperature and is given by

$$\lambda_w = 1.256\ \gamma^{1/2}\ \mu_w/\rho_w\ a_w .$$

ii) At the edge of the boundary layer, i.e. at $y = \delta$ :

$$u = u_e .$$

Based upon the hypersonic small disturbance theory, the tangential velocity at the edge of the boundary layer is equated with free-stream velocity, i.e.

$$u = u_e \simeq u_\infty \tag{2.6b}$$

(b) Boundary conditions for the energy equation :

i) At the surface of the wedge, i.e. at y = 0 :

$$H = H_b \tag{2.7a}$$

where $H_b$ is the enthalpy at the edge of the Knudsen layer.

ii) At the edge of the boundary layer, i.e. at y = $\delta$ :

$$H = H_e \simeq H_\infty \tag{2.7b}$$

The boundary condition (2.7a), in itself is incomplete, for the enthalpy at the edge of the Knudsen layer $H_b$ is still unknown. In the presence of slip it is observed that there exists a temperature jump across the Knudsen layer and the condition is

$$T_b - T_w = C_2 \lambda_w \left(\frac{\partial T}{\partial y}\right)_w \tag{2.8}$$

where $C_2$ is a constant found to depend on prandtl number, the ratio of specific heats and accommodation coefficient. This dependence is expressed as

$$C_2 = \frac{2\gamma}{\gamma+1} \frac{1}{Pr} \frac{2-\alpha}{\alpha} \tag{2.9}$$

and, for a wall with full accommodation at the surface (i.e., $\alpha = 1$) :

$$C_2 = \frac{2\gamma}{\gamma+1} \frac{1}{Pr}$$

$H_b$ in (2.7a) can now be evaluated in terms of $T_b$, (2.8) and $u_b$, (2.6a).

## §2.3 THE INTEGRAL EQUATIONS

Using continuity equation (2.1), a first integral of the momentum equation (2.2) may be written as

$$\frac{d}{dx} \int_0^\delta \rho u(u_\infty - u)\, dy = \frac{dP}{dx}\,\delta + \mu_w \left(\frac{\partial u}{\partial y}\right)_w \qquad (2.10)$$

Similarly the integral energy equation is :

$$\frac{d}{dx} \int_0^\delta \rho u(H-H_\infty)\, dy = -\left[\frac{\mu_w}{Pr}\left(\frac{\partial H}{\partial y}\right)_w + \left(1 - \frac{1}{Pr}\right)\mu_w \left(\frac{\partial}{\partial y}\frac{1}{2}u^2\right)_w\right] \qquad (2.11)$$

## §2.4 THE VELOCITY AND ENTHALPY PROFILES

The distribution of the tangential velocity component across the boundary layer is expressed as

$$\frac{u}{u_\infty} = k_1 + k_2 y$$

where $k_1$ and $k_2$ are constants. These constants, when determined by satisfying the boundary conditions at the surface, (2.6a) and the edge of the boundary layer, (2.6b), yield the following linear velocity profile.

$$\bar{u} = \frac{u}{u_\infty} = \frac{C_1 \lambda_w + y}{C_1 \lambda_w + \delta} . \qquad (2.12)$$

The variation of enthalpy across the boundary layer is represented by a second degree profile. This is compatible with the chosen velocity profile as $H \sim O(u^2)$.

Let,

$$\bar{H} = \frac{H}{H_\infty} = A + By + Cy^2 \qquad (2.13)$$

where A, B and C are constants which are implicitly functions of x. Equation (2.13), when subjected to the boundary condition (2.7a) gives

$$A = \frac{H_b}{H_\infty} = \bar{H}_b \ .$$

Using the relations

$$\left.\begin{aligned} H_b &= C_p\, T_b + \frac{1}{2}\, u_b^2 \\ H_w &= C_p\, T_w \end{aligned}\right] \qquad (2.14)$$

and evaluating the gradients of enthalpy and velocity from the respective profiles (2.12) and (2.13), one can re-write the temperature-jump condition (2.8) in the form

$$A = \bar{H}_b = \bar{H}_w + \frac{1}{2}\frac{u_\infty^2}{H_\infty}\left(\frac{C_1 \lambda_w}{C_1 \lambda_w + \delta}\right)^2 + C_2 \lambda_w \left[B - \frac{u_\infty^2}{H_\infty}\frac{C_1 \lambda_w}{(C_1 \lambda_w + \delta)^2}\right] \qquad (2.15)$$

where, for a hypersonic flow

$$\frac{u_\infty^2}{H_\infty} \simeq 2 \ .$$

Further, as $\left(\frac{\lambda_w}{\delta}\right)$ is a very small quantity, higher order terms have been left out. This approximation is justified even

for the extreme cases when $\bar{H}_w$ tends to zero, because a decrease in $\bar{H}_w$ would mean to increase B ($= \frac{1}{H_\infty} \frac{dH}{dy}|_w$) and B becomes appreciably large when $\bar{H}_w$ reaches zero. Thus, in either cases (i.e. adiabatic as well as fully cold wall) the error introduced in the formulation due to this approximation is not appreciable.

Thus,

$$A = \bar{H}_w + C_2 \lambda_w B$$

By satisfying the second boundary condition (2.7b), one obtains

$$C = \frac{1}{\delta^2} \left[ 1 - \bar{H}_w - C_2 \lambda_w B - \delta \right] .$$

Hence the enthalpy profile takes the final shape.

$$\bar{H} = (\bar{H}_w + C_2 \lambda_w B) + B y + \frac{1}{\delta^2} \left[ 1 - \bar{H}_w - B(C_2 \lambda_w + \delta) \right] y^2 \qquad (2.16)$$

Now we have obtained the two expressions for the velocity and enthalpy profiles with $\delta$ and B as unknowns. The coupled momentum and energy equations with substitution of these expressions are solved for these two unknowns.

## §2.5. THE MOMENTUM EQUATION - A WORKING FORM

Equation (2.3a) together with the equation of state (2.4) is used to express the density $\rho$ in terms of P, $\bar{H}$ and $\bar{u}$ i.e.,

$$\rho = \frac{\gamma P}{(\gamma - 1) H_\infty (\bar{H} - \bar{u}^2)} \qquad (2.17)$$

The momentum integral equation (2.10), after substituting for the density, $\rho$ from (2.17) gives

$$\frac{d}{dx}\int_0^{\delta}\frac{\gamma P}{\gamma-1}\frac{u_\infty^2}{\bar{H}_\infty}\frac{\bar{u}(1-\bar{u})}{\bar{H}-\bar{u}^2})\,dy = \frac{dP}{dx}\delta + \frac{\mu_w u_\infty}{C_1\lambda_w+\delta}\,.$$

Substituting for $\bar{u}$ and $\bar{H}$ from (2.12) and (2.16) and cancelling the common factor $(1 - y/\delta)$ from numerator and denomenator, the equation takes the form :

$$\frac{d}{dx}\int_0^{\delta}\left\{\frac{2\gamma P\delta^2}{(\gamma-1)(C_1\lambda_w+\delta)^2}\;\frac{(C_1\lambda_w+y)}{(\bar{H}_w+C_2\lambda_w)+\left[\bar{H}_w+B(C_2\lambda_w+\delta)\right]y}\right\}dy$$

$$= \frac{dP}{dx}\delta + \frac{\mu_w u_\infty}{C_1\lambda_w+\delta}\,.$$

This equation is simplified further by noting that

$$\frac{\delta^2}{(C_1\lambda_w+\delta)^2} = \frac{1}{(1+\frac{C_1\lambda_w}{\delta})^2} = \frac{1}{1+2C_1(\frac{\lambda_w}{\delta})+C_1^2(\frac{\lambda_w}{\delta})^2} \tilde{\sim} 1 \text{ as } \frac{\lambda_w}{\delta} \ll 1. \qquad (2.17a)$$

The above approximation has been made to facilitate the integration and we get,

$$\frac{d}{dx}\int_0^{\delta}\left\{\frac{2\gamma P}{(\gamma-1)}\;\frac{(C_1\lambda_w+y)}{(\bar{H}_w+C_2\lambda_w B)\delta+\left[\bar{H}_w+B(C_2\lambda_w+\delta)\right]y}\right\}dy$$

$$= \frac{dP}{dx}\delta + \frac{\mu_w u_\infty}{(C_1\lambda_w+\delta)}\,.$$

In this equation, P, B, and $\delta$ are functions of x only and hence, these may be taken out of the integral sign. The resultant equation may now be integrated to yield

$$\frac{d}{dx}\left\{\frac{2\gamma P}{(\gamma-1)\left[\bar{H}_w+C_2\,\lambda_w+\delta\right]B}\left[\delta-\frac{\bar{H}_w(\delta-C_1\,\lambda_w)+(C_1-C_2)B\delta\,\lambda_w}{\bar{H}_w+B(C_2\,\lambda_w+\delta)}\right.\right.$$

$$\left.\left.\ln\left(\frac{2(\bar{H}_w+C_2\,\lambda_w\,B)+B\delta}{(\bar{H}_w+C_2\,\lambda_w\,B)}\right)\right]\right\}=\frac{dP}{dx}\,\delta+\frac{\mu_w\,u_\infty}{(C_1\,\lambda_w+\delta)} \qquad (2.18)$$

The logarithmic term in the above equation is simplified by expanding it in a series form and neglecting the higher order terms. Thus, after some algebraic simplification the momentum equation (2.18) is simplified to :

$$\frac{d}{dx}\left\{\frac{2\gamma P\delta}{\gamma-1}\,\frac{1}{3(\bar{H}_w+C_2\,\lambda_w\,B)+B\delta}\right\}=\frac{dP}{dx}\,\delta+\frac{\mu_w\,u_\infty}{C_1\,\lambda_w+\delta} \qquad (2.19)$$

Equation (2.19) is next differentiated and the coefficients of derivatives are grouped together, leaving terms of order $\left(\frac{\lambda_w}{\delta}\right)^2$, $\frac{\lambda_w}{\delta}\frac{d\delta}{dx}$ and smaller.

$$P\left\{3(\bar{H}_w+C_2\,\lambda_w B)\left(\frac{d\delta}{dx}\right)-\delta^2\left(\frac{dB}{dx}\right)\right\}+\delta\left[3(\bar{H}_w+C_2\,\lambda_w B)+B\delta\right]$$

$$\left\{1-\frac{\gamma-1}{2\gamma}\left[3(\bar{H}_w+C_2\,\lambda_w\,B)+B\delta\right]\right\}\left(\frac{dP}{dx}\right)$$

$$=\frac{\gamma-1}{2\gamma}\left[3\,(\bar{H}_w+C_2\,\lambda_w\,B)+B\delta\right]^2+\frac{\mu_w\,u_\infty}{C_1\,\lambda_w+\delta} \qquad (2.20)$$

A particular case of equation (2.20) for adiabatic wall is obtained by putting $\bar{H}_w = 1$, $B = 0$, and by putting $\frac{2}{3}\gamma \approx 1$, one gets

$$2P \frac{d\delta}{dx} + \delta \frac{dP}{dx} = \frac{\mu_w u_\infty}{C_1 \lambda_w + \delta} \quad . \tag{2.21}$$

In the method developed by Kumar and Jain [24] for the flow over an insulated wedge, the above form of the momentum equation was used.

The range of validity of the equation (2.20), depends on how the pressure and its derivatives are prescribed. We first use the leading term of the tangent-wedge approximation, which is valid for the strong interaction region only :

$$\left.\begin{aligned} \frac{P}{P_\infty} &= \frac{\gamma(\gamma+1)}{2} M_\infty^2 (\beta + \frac{d\delta}{dx})^2 \\ \text{or} \quad P &= \frac{\gamma+1}{2} \rho_\infty u_\infty^2 (\beta + \frac{d\delta}{dx})^2 \\ \text{and} \quad \frac{dP}{dx} &= (\gamma+1) \rho_\infty u_\infty^2 (\beta + \frac{d\delta}{dx}) \frac{d^2\delta}{dx^2} \end{aligned}\right] \tag{2.22}$$

Substituting the expression contained in (2.22) into equation (2.20), one obtains,

$$\left[ 3(\bar{H}_w + C_2 \lambda_w B) \frac{d\delta}{dx} - \delta^2 \frac{dB}{dx} \right] (\beta + \frac{d\delta}{dx})^2 + 2\delta \left[ 3(\bar{H}_w + C_2 \lambda_w B) + B\delta \right]$$

$$\left\{ 1 - \frac{\gamma-1}{2\gamma} \left[ 3(\bar{H}_w + C_2 \lambda_w B) + B\delta \right] \right\} (\beta + \frac{d\delta}{dx}) \frac{d^2\delta}{dx^2}$$

$$= \frac{\gamma-1}{\gamma(\gamma+1)} \left[ 3(\bar{H}_w + C_2 \lambda_w B) + B\delta \right]^2 \frac{\mu_w}{\rho_\infty u_\infty} \frac{1}{C_1 \lambda_w + \delta} \tag{2.23}$$

Next the various variables are non-dimensionalized as given below :

We first notice that the ratio, $\mu_w/\rho_\infty u_\infty$, has the dimension of length. This ratio is denoted by L and has been used for non-dimensionalising the various quantities of interest.

$$\left.\begin{aligned} \eta &= \frac{\delta}{L} \\ \xi &= \frac{x}{L} \\ \psi &= BL \\ \therefore \quad \frac{d\delta}{dx} &= \frac{d\eta}{d\xi} = \eta' \\ \frac{d^2\delta}{dx^2} &= \frac{1}{L}\frac{d^2\eta}{d\xi^2} = \frac{1}{L}\eta'' \\ \frac{dB}{dx} &= \frac{1}{L^2}\frac{d\psi}{d\xi} = \frac{1}{L^2}\psi' \end{aligned}\right\} \quad (2.24)$$

and

$$B\delta = \eta\psi$$

Also, let us define the two strong-interaction slip parameters $e_{11}$ and $e_{22}$ as :

$$\left.\begin{aligned} {}^{\dagger}e_{11} &= \frac{C_1 \lambda_w}{L}(\beta + \eta')^2 = \left(\frac{1.256}{\gamma+1}\right) C_1 \left[\frac{2(\gamma-1)}{\gamma}\bar{H}_w\right]^{1/2} \\ {}^{\dagger}e_{22} &= \left(\frac{C_2 \lambda_w}{L}\right)(\beta + \eta')^2 = \left(\frac{1.256}{\gamma+1}\right) C_2 \left[2\frac{(\gamma-1)}{\gamma}\bar{H}_w\right]^{1/2} \end{aligned}\right\} \quad (2.25)$$

Equation (2.25) shows that under an extreme cold wall situation (i.e. $\bar{H}_w = 0$), the phenomenon of slip is apparently absent. Insertion of the expressions (2.24) and (2.25) in eq.(2.23) leads to

† See appendix .

$$\left[3(\bar{H}_w+\psi_{22})\ \eta' - \eta^2\ \psi'\right](\beta+\eta')+\eta\eta''\left[3(\bar{H}_w+\psi_{22})+\eta\psi\right]$$

$$\left\{2-\frac{\gamma-1}{\gamma}\left[3(\bar{H}_w+\psi_{22})+\eta\psi\right]\right\}$$

$$=\frac{\gamma-1}{\gamma(\gamma+1)}\left[3(\bar{H}_w+\psi_{22})+\eta\psi\right]^2\times\frac{(\beta+\eta')}{\left[e_{11}+\eta(\beta+\eta')^2\right]} \tag{2.26}$$

where

$$\psi_{22}=\frac{e_{22}\,\psi}{(\beta+\eta')^2} \tag{2.27}$$

Equation (2.26) gives a particular case of adiabatic wall with $\bar{H}_w = 1$, and $\psi = 0$, like

$$e_{11}\left[\eta'(\eta'+\beta)+\eta\eta''\right]+\eta\eta'\ (\eta'+\beta)^3+\eta^2\eta''\ (\eta'+\beta)^2=\frac{1}{\gamma+1}\ (\eta'+\beta) \tag{2.28}$$

This was the equation used by Kumar and Jain [24] for the analysis of hypersonic flow over insulated wedges with $e_{11}$ here identically equal to e.

The pressure and its derivatives in the equation (2.20) are now represented by a full tangent-wedge approximation thereby, extending the range of validity of the analysis to weak-interaction zone also. The full tangent-wedge approximation is expressed as

$$\frac{P}{P_\infty}=\left\{1+\gamma k\left[\sqrt{1+b^2k^2}+bk\right]\right\}$$

or

$$P = \frac{\rho_\infty u_\infty^2}{\gamma M_\infty^2}\{1 + (\gamma k)\left[\sqrt{1+b^2k^2} + bk\right]\}$$

and

$$\frac{dP}{dx} = \frac{\rho_\infty u_\infty^2}{M_\infty}\{2\left[\sqrt{1 + b^2 k^2} + bk\right] - \frac{1}{\sqrt{1+b^2k^2}}\}\left(\frac{d^2\delta}{dx^2}\right)$$

(2.29)

where

$$k = M_\infty\left(\beta + \frac{d\delta}{dx}\right)$$

and $$b = \frac{\gamma+1}{4}$$

(2.30)

Here also we define the following two slip parameters $e_1$ and $e_2$ :

$$e_1 = 1.256\, C_1 \sqrt{\frac{\gamma(\gamma-1)}{2}\bar{H}_w}$$

and $$e_2 = 1.256\, C_2 \sqrt{\frac{\gamma(\gamma-1)}{2}\bar{H}_w}$$

(2.31)

Also we can see

$$\frac{{}^{\dagger}C_1\,\lambda_w}{L} = e_1\,\omega$$

and $$\frac{{}^{\dagger}C_2\,\lambda_w}{L} = e_2\,\omega$$

(2.32)

where

$$\omega = \frac{M_\infty^2}{P/P_\infty}$$

---

† See appendix

or, from equation (2.29),

$$\omega = M_\infty^2 / \{1 + \gamma k \left[ \sqrt{1 + b^2 k^2} + b k \right]\} \qquad (2.33)$$

Equation (2.29) through (2.33) are now substituted in equation (2.20) after non-dimensionalising it with the help of relations given by (2.24). Thus we obtain final working form of the momentum equation which incorporates the effects of both slip and heat transfer.

$$\left[ 3(\bar{H}_w + e_2 \omega\psi)\, \eta' - \eta^2 \psi' \right] \{1 + \gamma k \left[ \sqrt{1+b^2k^2} + bk \right]\} + \eta\eta'' \left[ 3(\bar{H}_w + e_2 \psi\omega) + \eta\psi \right]$$

$$\{1 - \frac{\gamma - 1}{2\gamma} \left[ 3(\bar{H}_w + e_2 \omega\psi) + \eta\psi \right]\} \{2\gamma M_\infty \left[ \sqrt{1+b^2k^2} + bk \right] - \frac{\gamma M_\infty}{\sqrt{1+b^2k^2}}\}$$

$$= \frac{\gamma - 1}{2} M_\infty^2 \left[ 3(\bar{H}_w + e_2 \omega\psi) + \eta\psi \right]^2 \frac{1}{(\eta + e_1 \omega)} \qquad (2.34)$$

A particular case of equation (2.34) for insulated wedges with $\bar{H}_w = 1$ and $\psi = 0$ results in an equation which is exactly similar to Chowdhary's [25] equation with full tangent-wedge approximation for adiabatic surfaces.

## §2.6 THE ENERGY EQUATION - A WORKING FORM

The energy integral equation (2.11), after substituting for the density from (2.17) and the gradients of enthalpy and velocity from (2.12) and (2.16), takes the form

$$\frac{d}{dx} \int_0^\delta \frac{\gamma P}{(\gamma - 1)} u_\infty \frac{\bar{u}(\bar{H} - 1)}{(\bar{H} - \bar{u}^2)} dy = - \frac{\mu_w}{Pr} B H_\infty - (1 - \frac{1}{Pr}) u_\infty^2 \frac{C_1 \lambda_w}{(C_1 \lambda_w + \delta)^2} \qquad (2.35)$$

Substituting for $\bar{u}$ and $\bar{H}$ from (2.12) and (2.17) and neglecting terms of order $(\frac{\lambda_w}{\delta})^2$ or smaller, equation (2.35) is transformed after the algebraic simplifications to a form more amenable for a closed form integration in the normal direction as,

$$\frac{d}{dx}\int_0^{\delta}\left\{\frac{\gamma P\, u_\infty}{(\gamma-1)\delta}\,\frac{\left[\bar{H}_w+(C_2\lambda_w+\delta)B-1\right]}{\left[\bar{H}_w+(C_2\lambda_w+\delta)B\right]}\times\left(\frac{y^2+my}{y+n}\right)\right\}dy$$

$$=-\frac{\mu_w}{Pr}B\,H_\infty-\left(1-\frac{1}{Pr}\right)\frac{u_\infty^2\,C_1\lambda_w}{(C_1\lambda_w+\delta)^2} \qquad (2.36)$$

where

$$m=\frac{(\bar{H}_w+C_2\lambda_w B-1)\,\delta}{\left[\bar{H}_w+B(C_2\lambda_w+\delta)-1\right]}$$

and

$$n=\frac{(\bar{H}_w+C_2\lambda_w)\,\delta}{\left[\bar{H}_w+(C_2\lambda_w+\delta)B\right]} \qquad (2.37)$$

After carrying out the integration equation, (2.36) yields :

$$\frac{d}{dx}\left\{\frac{\gamma P\, u_\infty}{(\gamma-1)\delta}\,\frac{\left[\bar{H}_w+(C_2\lambda_w+\delta)B-1\right]}{\left[\bar{H}_w+(C_2\lambda_w+\delta)B\right]}\left[\frac{\delta^2}{2}+(m-n)\delta+n(n-m)\ln\left(\frac{\delta+n}{\delta}\right)\right]\right\}$$

$$=-\frac{\mu_w}{Pr}B\,H_\infty-\left(1-\frac{1}{Pr}\right)\frac{u_\infty^2\,C_1\lambda_w}{(C_1\lambda_w+\delta)^2} \qquad (2.38)$$

The logarithmic term in the above equation is simplified by expanding it in a series form and neglecting the higher order smaller terms :

$$\ln\left(\frac{\delta+n}{\delta}\right) \simeq 2\left\{\frac{\bar{H}_w + (C_2\lambda_w + \delta)B}{3(\bar{H}_w + C_2\lambda_w B) + B\delta}\right\} \qquad (2.39)$$

Upon insertion of equations (2.37) and (2.39) in eq.(2.38) and after considerable algebraic rearrangements and simplifications,

We obtain for equation (2.38),

$$\frac{d}{dx}\left\{\frac{\gamma P u_\infty \delta}{2(\gamma-1)} \frac{3(\bar{H}_w + C_2\lambda_w B - 1) + B\delta}{3(\bar{H}_w + C_2\lambda_w) + B\delta}\right\} = -\frac{\mu_w}{Pr} B H_\infty$$

$$- \left(1 - \frac{1}{Pr}\right)\mu_w u_\infty^2 \frac{C_1\lambda_w}{(C_1\lambda_w + \delta)^2} \qquad (2.40)$$

Carrying out the differentiation in equation (2.40) and grouping the coefficients of derivatives together, one obtains,

$$\frac{\gamma u_\infty}{2(\gamma-1)}\left\{P\left[\left\{\left[3(\bar{H}_w + C_2\lambda_w B) + B\delta\right]^2 - 9(\bar{H}_w + C_2\lambda_w B)\right\}\left(\frac{d\delta}{dx}\right)\right.\right.$$

$$+ 3\delta(3C_2\lambda_w + \delta)\frac{dB}{dx}\left]\left[3(\bar{H}_w + C_2\lambda_w B) + (B\delta - 3)\right]\delta\right.$$

$$\left.\left[3(\bar{H}_w + C_2\lambda_w B) + B\delta\right]\left(\frac{dP}{dx}\right)\right\}$$

$$= -\frac{\mu_w}{Pr} B H_\infty - \left(1 - \frac{1}{Pr}\right)\mu_w u_\infty^2 \frac{C_1\lambda_w}{(C_1\lambda_w + \delta)^2} \qquad (2.41)$$

The pressure and its derivatives appearing in eq. (2.41) are first described by a tangent-wedge approximation valid for the strong interaction region given by the expression (2.22). The equation is non-dimensionalised by employing a scheme similar to (2.24). The slip parameters employed here are the same as

those given by expression (2.25). Thus with the substitution of equations (2.22), (2.24) and (2.25) in equation (2.41), we obtain the energy equation for the strong interaction region in its final form as :

$$(\beta+\eta')^2 \{ \eta' [ \{ 3(\bar{H}_w + \psi_{22}) + \eta\psi \}^2 - 9(\bar{H}_w + \psi_{22}) ] + 3\eta\psi' \left(\frac{3e_2}{(\beta+\eta')} + \eta\right) \} \cdot$$

$$+ 2\eta\eta''(\beta+\eta') [ 3(\bar{H}_w+\psi_{22})+\eta\psi ] [ 3(\bar{H}_w+\psi_{22})+\eta\psi-3 ]$$

$$= -\frac{4(\gamma-1)}{\gamma(\gamma-1)} [ 3(\bar{H}_w+\psi_{22})+\eta\psi ]^2 \left[ \frac{\psi}{2Pr} + \left(1 - \frac{1}{Pr}\right) \frac{e_{11}(\beta+\eta')^2}{e_{11} + \eta(\beta+\eta')^2} \right] \tag{2.42}$$

where $\psi_{22}$ is defined as given by (2.27).

We now extend equation (2.41) with the help of full tangent-wedge approximation given by expression (2.29). Non-dimensionalising the equation (2.41) in the same way as equation (2.24) we obtain

$$\{ [ [ 3(\bar{H}_w+e_2\omega\psi)+\eta\psi ]^2 - 9(\bar{H}_w+e_2\omega\psi) ] \eta' + 3\eta(3e_2\omega+\eta) \psi' \}$$

$$\{ 1+\gamma k [ \sqrt{1+b^2k^2}+bk ] \} + \eta\eta'' [ 3(\bar{H}_w+e_2\omega\psi)+\eta\psi ] [ 3(\bar{H}_w+e_2\omega\psi)$$

$$+ \eta\psi - 3 ] \{ 2\gamma M_\infty [ \sqrt{1+b^2k^2}+bk ] - \frac{\gamma M_\infty}{\sqrt{1+b^2k^2}} \}$$

$$= -2(\gamma-1)M_\infty^2 [ 3(\bar{H}_w+e_2\omega\psi)+\eta\psi ]^2 \left[ \frac{\psi}{2.Pr} + \left(1 - \frac{1}{Pr}\right) \frac{e_1\omega}{(e_1\omega+\eta)^2} \right] \tag{2.43}$$

where k is given by (2.30), and $e_1$ and $e_2$ are given by (2.31), and $\omega$ is given by (2.33).

Equation (2.43) represents the final working form of the energy equation which incorporates the effects of both slip and temperature-jump and is valid for the strong interaction region as well as for the weak interaction zone.

Thus, we have the two equations, namely, the momentum (2.34) and the energy (2.43), which are coupled and solved simultaneously for the unknowns $\eta$ , the non-dimensionalised boundary layer thickness and $\psi$ , the non-dimensionalised enthalpy gradient.

## §2.7. WORKING EQUATIONS FOR NO-SLIP CASE

The governing equations for the no-slip case are derived as a particular case from those for the slip case, with the slip parameters equated to zero. Thus the momentum and energy equations for strong interaction regions for no slip case are obtained from (2.26) and (2.42) by putting $e_{11} = e_{22} = \psi_{22} = 0$.

Momentum :

$$(3\bar{H}_w\ \eta' - \eta^2\ \psi')\ (\beta + \eta') + \eta\eta''\ (3\bar{H}_w + \eta\psi)\left[2 - \frac{\gamma-1}{\gamma}(3\bar{H}_w+\eta\psi)\right]$$

$$= \frac{\gamma-1}{\gamma(\gamma+1)}\ (3\bar{H}_w + \eta\psi)^2\ \frac{1}{\eta(\beta+\eta')} \qquad (2.44)$$

Energy :

$$(\beta+\eta')^2 \{ [ (3H_w+\eta\psi)^2-9\bar{H}_w ] \eta' + 3\eta^2 \psi' \} + 2\eta\eta'' (\beta+\eta')(3\bar{H}_w+\eta\psi-3)$$

$$= - \frac{2(\gamma-1)}{\gamma(\gamma+1)} \frac{\psi}{Pr} (3\bar{H}_w + \eta\psi)^2 \qquad (2.45)$$

The respective equations for no-slip flow situation with the induced pressure and its gradient described by a full tangent-wedge approximation may also be derived from the corresponding equations for slip case.

Thus, with $e_1 = e_2 = 0$, equation (2.34) gives the momentum equation for no-slip case.

$$(3\bar{H}_w \eta' - \eta^2 \psi') \{1 + \gamma k [ \sqrt{1+b^2k^2}+bk ] \} + \eta\eta'' (3\bar{H}_w + \eta\psi)$$

$$[ 1 - \frac{\gamma-1}{2\gamma} (3\bar{H}_w + \eta\psi) ] \{ 2\gamma M_\infty [ \sqrt{1+b^2k^2}+bk ] - \frac{\gamma M_\infty}{\sqrt{1+b^2k^2}} \}$$

$$= \frac{\gamma-1}{2} M_\infty^2 (3\bar{H}_w + \eta\psi)^2 \frac{1}{\eta} \qquad (2.46)$$

The energy equation is obtained from equation (2.43) as :

$$\{ [ (3\bar{H}_w + \eta\psi)^2 - 9\bar{H}_w ] \eta' + 3\eta^2 \psi' \} \{ 1 + \gamma k [ \sqrt{1+b^2k^2}+bk ] \}$$

$$+ \eta\eta'' (3\bar{H}_w + \eta\psi) [ 3(\bar{H}_w-1) + \eta\psi ] \{ 2\gamma M_\infty [ \sqrt{1+b^2k^2}+bk ]$$

$$- \frac{\gamma M_\infty}{\sqrt{1+b^2k^2}} \} = - \frac{(\gamma-1)M_\infty^2}{Pr} \psi (3\bar{H}_w + \eta\psi)^2 \qquad (2.47)$$

# CHAPTER III

## METHOD OF SOLUTION

In this chapter we present the solutions to the two ordinary second order equations (2.34) and (2.43) with slip and temperature-jump boundary conditions. Solutions will also be given for equations (2.46) and (2.47) without slip at the boundary. For both slip and no-slip cases integration of the complete momentum and energy equations is not possible due to the lack of initial conditions. Hence an analytical solution is provided by solving the strong-interaction equations by a series-solution procedure. This provides the initial conditions for the numerical integration of the governing equations when the full-tangent wedge approximation is employed, for obtaining the solution from strong to weak interaction regimes. The no slip equations (2.46) and (2.47) are singular in nature at the leading edge ($\xi = 0$), hence the integration of these equations is started from a point slightly away from leading edge. However, in slip case the integration may be started from the leading edge itself.

### §3.1 ANALYTICAL SOLUTION FOR SLIP CASE

The momentum equation (2.26) and energy equation (2.42) for the strong-interaction region is now solved by a series-solution procedure.

We express $\eta$ and $\psi$ as :

$$\left.\begin{aligned} \eta &= \xi^{\sigma} \sum_{n=0}^{\infty} a_n \xi^{nq} \\ \psi &= \xi^{p} \sum_{n=0}^{\infty} b_n \xi^{ns} \end{aligned}\right] \qquad (3.1)$$

Therefore,

$$\left.\begin{aligned} \eta' &= \xi^{\sigma-1} \sum_{n=0}^{\infty} a_n (\sigma + nq) \xi^{nq} \\ \eta'' &= \xi^{\sigma-2} \sum_{n=0}^{\infty} a_n (\sigma + nq)(\sigma + nq - 1) \xi^{nq} \\ \psi' &= \xi^{p-1} \sum_{n=0}^{\infty} b_n (p + ns) \xi^{ns} \end{aligned}\right] \qquad (3.2)$$

Next, the expressions given by (3.1) and (3.2) are substituted in the equations (2.26) and (2.42). Collecting the terms of like powers of $\xi$ , we notice that for a compatible series and for slip to be a dominant phenomenon at the leading edge

$$\left.\begin{aligned} &\sigma = 1, \; q = 1 \\ \text{and} \\ &p = 0, \; s = 1 \end{aligned}\right] \qquad (3.3)$$

Thus,

$$\left.\begin{aligned} \eta &= a_0 \xi + a_1 \xi^2 + a_2 \xi^3 \\ \psi &= b_0 + b_1 \xi + b_2 \xi^2 \end{aligned}\right] \qquad (3.4)$$

Therefore,

$$\eta'|_{\xi=0} = a_o \ , \quad \eta''|_{\xi=0} = 2a_1$$

and

$$\psi|_{\xi=0} = b_o \ , \quad \psi'|_{\xi=0} = b_1$$

The coefficients $a_o$ and $b_o$ can be found directly from the equations (2.26) and (2.42). We also notice that at $\xi = 0$, $\eta = 0$.

The momentum equation (2.26) at $\xi = 0$ yields

$$b_o = \psi|_{\xi=0} = \frac{(\beta+\eta')^2}{3(\gamma-1)\, e_{22}} \left[ \gamma(\gamma+1)\, e_{11}\, \eta' - 3(\gamma-1)\, \bar{H}_w \right] \tag{3.5}$$

where in expression (3.5) $\eta'$ is evaluated at the leading edge. The energy equation (2.42) at $\xi = 0$, in conjunction with (3.5), gives

$$a_o = \eta'|_{\xi=0} = \left[ 1 + \frac{2}{3} \frac{e_{11}\, \bar{H}_w}{e_{22}\, Pr} - \frac{4}{3} \left(1 - \frac{1}{Pr}\right) \Big/ \frac{\gamma(\gamma+1)}{3(\gamma-1)}\, e_{11} \left(1 + \frac{2e_{11}}{3e_{22} Pr}\right) \right] \tag{3.6}$$

Expressions (3.5) and (3.6) jointly give $a_o$ and $b_o$ as a function of $\gamma$, $e_{11}$, $e_{22}$, Pr and $\bar{H}_w$; all of these are already specified.

$a_1$ and $b_1$ are found by equating the coefficients of $\xi$ in the momentum and energy equations. Thus the momentum and energy equations (2.26) and (2.42) respectively give :

$$a_1 = \frac{\alpha_1 \alpha_4 - \alpha_2 \alpha_3}{\alpha_1 - \alpha_3}$$

and

$$b_1 = \frac{\alpha_4 - \alpha_2}{\alpha_1 - \alpha_3} \qquad (3.7)$$

where

$$\alpha_1 = \frac{3e_{22}\, f}{r}\left[2g - (\gamma+1)\, a_o\, e_{11}\, f^2\right]$$

$$\alpha_2 = \frac{a_o\, g\, f^3}{r}\left[2b_o - 3(\gamma+1)\, a_o\, f^2\right]$$

$$\alpha_3 = -\frac{6g}{s}\left\{e_{11}^2\left[3(\gamma+1)e_{22}\, f^2 + \frac{e_{11}^2\, g}{Pr}\right] + 4e_{22}\, h\right\}$$

$$\alpha_4 = -\frac{a_o g f^2}{s}\left\{4b_o\left(\frac{3e_{11}g}{Pr} + 2h\right) + 6a_o e_{11} f^2(\gamma+1)\right.$$
$$\left.\left[3\,(g - f^2\bar{H}_w) - e_{11}\, b_o\right]\right\} \qquad (3.8)$$

In the above expressions, the various symbols have the following meaning :

$$r = g\left\{f^2\left[6e_{11}(f+a_o)(\gamma+1) + 24(\gamma+1)e_{11}\, a_o - 24\bar{H}_w\right]\right.$$
$$\left. - 6g\left[1 + a_o\, e_{11}\,(\gamma+1)\right]\right\} + 12a_o\, e_1\, a^4\, \bar{H}_w$$

$$s = 18(\gamma+1)\, f\, e_{11}^2\left[f^2\, \bar{H}_w\,(3 - f - 4a_o) + g^2\right] + 96f\, g\, h\, \bar{H}_w$$
$$+ (\gamma+1)\, e_{11}\, g\,\left(1 - \frac{1}{Pr}\right) \qquad (3.9)$$

$$f = (\beta + a_o)$$

$$g = \bar{H}_w(\beta + a_o) + e_{22}\, b_o$$

$$h = \frac{b_o e_{11}^2}{2Pr} + \left(1 - \frac{1}{Pr}\right) e_{11} (a_o + \beta)^2. \qquad (3.9)$$

Thus, the equation (3.4) supplemented by equations (3.5) through (3.9) gives the leading-edge solution.

The analytical solutions developed are compared with those by Kumar and Jain [24] for the adiabatic slip case.

For adiabatic surface with $\psi = 0$ and $\bar{H}_w = 1$, relation (3.5) gives

$$a_o = \eta'|_{\xi=0} = \frac{1}{(\gamma+1)\, e_{11}} \qquad (3.10)$$

$$b_o = 0$$

and, from (3.7),

$$a_1 = -\left(\frac{2}{\gamma+1}\right)^2 \left[\frac{2}{\gamma+1} + 2e_{11}\beta\right]^3 / 64 e_{11}^5 \left(\frac{2}{\gamma+1} + e_{11}\beta\right) \qquad (3.11)$$

$$b_1 = 0$$

Kumar and Jain [24] got the same values of $a_o$ and $a_1$ in their analysis as those given by (3.10) and (3.11), which serves as a check on the correctness of the analytical scheme developed.

## §3.2 ANALYTICAL SOLUTION FOR NO-SLIP CASE.

Unlike for slip flow, the basic equations for no slip flow are singular in nature at the leading edge of the wedge. For the slip case one can extract some of the initial information

from the equations itself and hence the series solution procedure is comparatively easier. However, for no-slip case no such information is available due to the singular nature of the equations, which further complicates the already tedious job. The equation which we solve here are the momentum equation (2.44) and the energy equation (2.45).

As for slip case, we use series expansion for $\eta$ and $\psi$ as given by the expression (3.1).

Substituting for $\eta$, $\eta'$, $\eta''$, $\psi$ and $\psi'$ from (3.1) and (3.2) in equations (2.44) and (2.45). We find that, for a compatible series,

$$\sigma = \frac{3}{4}, \quad q = \frac{1}{4}$$

and

$$p = \frac{-3}{4}, \quad s = \frac{1}{4}.$$

Therefore,

$$\left.\begin{aligned} \eta &= a_o \xi^{3/4} + a_1 \xi + a_2 \xi^{5/4} \\ \psi &= b_o \xi^{-3/4} + b_1 \xi^{-1/2} + b_2 \xi^{-1/4} \end{aligned}\right] \qquad (3.12)$$

where $a_o$ and $b_o$ in (3.12) are determined from the equations obtainined by equating the constant terms in the expanded momentum and energy equations.

$$\left(\frac{9}{64}\frac{\gamma-1}{\gamma}\right) a_o^6 b_o^2 + \left(\frac{54}{64}\frac{\gamma-1}{\gamma}\bar{H}_w + \frac{9}{64}\right) a_o^5 b_o + \left(\frac{81}{64}\frac{\gamma-1}{\gamma}\bar{H}_w^2 + \frac{27}{64}\bar{H}_w\right) a_o^4$$

$$- \frac{\gamma-1}{\gamma(\gamma+1)}\left[a_o^2 b_o^2 + 6\bar{H}_w a_o b_o + 9\bar{H}_w^2\right] = 0 \qquad (3.13)$$

$$\left(\frac{9}{64} a_o^6 b_o^3\right) + \left(\frac{54}{64}\bar{H}_w - \frac{27}{64}\right) a_o^5 b_o^2 - \frac{9}{64}\left(9\bar{H}_w + 11\bar{H}_w^2\right) a_o^4 b_o +$$

$$\left[\frac{54}{64}\left(\bar{H}_w - 1\right)\left(\bar{H}_w^2\right) + \frac{(2\gamma-1)b_o^4}{\gamma(\gamma+1)Pr}\right] a_o^3$$

$$+ \frac{2(\gamma-1)}{\gamma(\gamma+1)Pr}\left(6\bar{H}_w a_o b_o^2 + 11\bar{H}_w^2 a_o b_o + 6\bar{H}_w^2\right) = 0 \qquad (3.14)$$

Equations (3.13) and (3.14) are solved for $a_o$ and $b_o$ by the Newton-Raphson method. To start the Newton-Raphson iterations the range of variation of $a_o$ and $b_o$ are found for the two extreme cases of $\bar{H}_w = 1$ and $\bar{H}_w = 0$, and is given below :

| $\bar{H}_w$ | $a_o$ | $b_o$ |
|---|---|---|
| 0 | 0.87422 | 0.983014 |
| 1 | 1.0813928 | 0.0 |

Once $a_o$ and $b_o$ are found $a_1$ and $b_1$ are determined by equating the coefficients $\xi^{1/4}$ in the expanded momentum and energy equations :

$$\left.\begin{aligned} a_1 &= \frac{A_o B_2 - A_2 B_o}{A_1 B_o - A_o B_4} \\ b_1 &= \frac{A_2 B_1 - A_1 B_2}{A_1 B_o - A_o A_2} \end{aligned}\right] \qquad (3.15)$$

where

$$A_o = 6\,\frac{\gamma-1}{\gamma}\,a_o^5\left(\frac{3}{64}\,a_o b_o - \bar{H}_w\right) - \frac{\gamma-1}{\gamma(\gamma+1)}\,a_o\left(6\bar{H}_w + 2a_o b_o\right)$$

$$A_1 = \frac{a_o^3}{64}\left\{a_o b_o\left[48\,\frac{\gamma-1}{\gamma}\,a_o b_o + 243\,\bar{H}_w\,\frac{\gamma-1}{\gamma} + 57\right] + 270\,\frac{\gamma-1}{\gamma}\,\bar{H}_w + 225\right\} - \frac{\gamma-1}{\gamma(\gamma+1)}\,b_o\left(6\bar{H}_w + 2a_o b_o\right)$$

$$A_2 = \frac{12}{64}\,\beta a_o^3\left\{\frac{\gamma-1}{\gamma}\,a_o^2 b_o + a_o b_o\left(6\bar{H}_w\,\frac{\gamma-1}{\gamma} + 4\right) + \left(9\bar{H}_w^2\,\frac{\gamma-1}{\gamma} + 12\right)\right\}$$

$$B_o = \frac{a_o^4}{64}\left[a_o b_o\left(108\bar{H}_w + 27a_o b_o - 27\right) + \bar{H}_w\left(99\bar{H}_w - 63\right)\right] + \frac{2(\gamma-1)}{\gamma(\gamma+1)}\left\{4a_o^3 b_o^3 + 18\bar{H}_w a_o^2 b_o^2 + \bar{H}_w^2\left[11a_o\left(1+b_o\right) + 6\bar{H}_w\right]\right\}$$

$$B_1 = \frac{a_o^3 b_o}{64}\left[73a_o^2 b_o^2 + a_o b_o\left(504\bar{H}_w - 225\right) + \left(825\bar{H}_w - 657\right)\bar{H}_w\right] + \frac{396}{64}\,a_o^2\bar{H}_w^2\left(\bar{H}_w - 1\right) + \frac{2(\gamma-1)}{\gamma(\gamma+1)}\left[3a_o^2 b_o^4 + 11\bar{H}_w^2 b_o + 12\bar{H}_w\,a_o b_o^2\right]$$

$$B_2 = \frac{a_o^4}{16}\,\beta\,b_o\left\{a_o b_o\left[12b_o^2 + 6\left(3 - 6\bar{H}_w\right)b_o\right] + 6\bar{H}_w\left(9 - 11\bar{H}_w\right) + \left(108\bar{H}_w - 54\right)b_o\right\} + \frac{27}{4}\,a_o^2\,\beta\,\bar{H}_w\left(\bar{H}_w - 1\right)$$

(3.16)

This completes the leading edge solution for no slip case.

## §3.3. NUMERICAL INTEGRATION SCHEME

After developing the analytical solutions for leading edge we now solve equations (2.34) and (2.43) for slip case and

(2.46) and (2.47) for no-slip case, with the full tangent wedge approximation to get solutions which are valid from strong to weak interaction regions covering the transition region.

Integration is started from the leading edge ($\xi = 0$) for the slip case and from a point slightly away from the leading edge ($\xi = 0.10$) for the no-slip case. A fourth-order Runge-Kutta algorithm is used to start the integration. After the fourth step, integration is proceeded by employing 'Milne's Predictor' followed by 'Hamming's Corrector' formulae. The predicted value is modified by assuming that the local truncation error on successive intervals does not change appreciably. A provision for the correction of truncation error is also given. These modifications and corrections enhance the convergence. Step-size at the start is taken as 0.025 and is increased by tenfold after every eighty steps. Also after every eighty steps, the Runge-Kutta method is used again to proceed through the next four steps and thereafter is followed by the predictor-corrector method. This procedure avoids the chances of the errors getting magnified and also enables a faster convergence.

The various formulae used in the numerical integration are :

(a) Fourth order Milne's predictor formula :

$$y_{i+1,0} = y_{i-3} + \frac{4}{3} h \, (2f_i - f_{i-1} + 2f_{i-2}) \qquad (3.17)$$

(b) Modification for the predicted value is obtained from :

$$y^{*}_{i+1,0} = y_{i+1,0} + \frac{112}{121}(y_{i,k} - y_{i,0}) \qquad (3.18)$$

(c) Hamming's Corrector equation

$$y^{j+1}_{i+1} = \frac{1}{8}\{9y_i - y_{i-2} + 3h[f(x_{i+1}, y^{j}_{i+1}) + 2f_i - f_{i-1}]\} \qquad (3.19)$$

$$j = 0,1,2,\ldots,(k-1).$$

(d) Correction for truncation error is given by :

$$y_{i+1} = y_{i+1,k} - \frac{9}{121}(y_{i+1,k} - y_{i+1,0}). \qquad (3.20)$$

where 'f' is the gradient of y in the direction in which the step 'h' is taken. Here 'i' is the step count and 'j' is the iteration count.

The solutions were obtained for various values of the free stream Mach number, semi-wedge angle, wall enthalpy ratios and Prandtl number.

Computations have been carried out on the IBM 7044/1401 computer at the I.I.T. Computer Centre. It is found that one set of computations requires a computer time in the range 1.5 to 2 minutes. On the other hand, a finite difference technique [26] requires a computer time not less than 30 minutes for one set of computations. Thus, the present method saves the computational time considerably.

# CHAPTER IV

## RESULTS AND DISCUSSIONS

In this chapter, the various results obtained in the present investigations and their comparison with the previous theoretical and experimental findings are discussed in detail. Briefly, the conclusions drawn therefrom are presented at the end of this chapter.

Fig. 2 shows the variation of the boundary layer thickness along a cold surface for semi-wedge angles of $0^{\circ}$, $2^{\circ}$ and $5^{\circ}$. It is seen that the boundary layer thickness holds an inverse relation with the wedge angle, which is true because a higher wedge angle causes an increased inviscid compression which, in turn, will have a tendency to keep the boundary layer thin. It is also seen that the boundary layer thickness is larger for $M_{\infty} = 10$ than for $M_{\infty} = 20$ for the same values of $\bar{x}_{\ell}$ and the semi-wedge angle. This behaviour is also attributed to the higher inviscid pressures at high Mach numbers which overcome the opposing effect of rarefaction at high speeds. Our results are in quite good agreement with those of Chattopadhyay [27] for semi-wedge angles of $0^{\circ}$ and $2^{\circ}$ and for Mach numbers 10 and 20 for no-slip case.

In fig. 3 a plot of $\bar{\delta}$ for various thermal conditions at the wall for both slip and no-slip cases is given. It can

be seen that $\bar{\delta}$ continues to decrease as the wall becomes cooler. This is expected because the density of the fluid in the boundary layer is maximum when the wall is fully cold. Again, for the same wall-enthalpy ratios, slightly lower results are obtained when the effect of rarefaction is incorporated. It is worth noticing that the difference between the slip and no-slip solutions becomes negligible at highly cooled surface conditions.

The surface pressure distribution as a function of $\bar{x}$ is shown in fig. 4 for different wall temperatures. We observe a reduced pressure level for a lower wall temperature. Similarly slip reduces the pressure level markedly towards the leading edge and much less at the downstream stations. This type of behaviour is due to the fact that, in a hypersonic stream, the effective thickness of the body decreases with decrease in wall temperature or slip. In fig. 4, present results are given for three wall conditions $\bar{H}_w = 0.5$, 0.15 and 0.065 with $M_\infty = 20$, $Pr = 0.75$ and $\beta = 0^\circ$ for slip and no-slip cases. For $\bar{H}_w = 0.065$, present results are compared with the experimental data of Vidal and Wittliff [28] and for $\bar{H}_w = 0.15$ a comparison is made with the data of Vas and McDougall [29]. A reasonable agreement is observed in these comparisons. The theoretical predictions of Cheng [13] for strong and weak interaction zones agree quite well with the present curves in the relevant regions. However, the present results are slightly lower than Menon's [26] finite difference solutions. Fig. 5 shows the

variation of wall pressure along the surface of a semi-cooled body for various wedge angles. It is seen that the pressure level increases with increase in wedge angle and Mach number. The results compare favourably with those of Chattopadhyay [27].

The variation of $C_f^{\wedge} = M_\infty^3 C_f/2\bar{x}^{3/2}$ with rarefaction parameter is shown in fig. 6 for four different cases of wall cooling, namely, $\bar{H}_w$ = 1.0, 0.5, 0.20 and 0.065. The skin friction is seen to decrease as the wall is progressively cooled, due to the reduction in the coefficient of viscosity. For the same wall conditions a lesser skin friction is noticed for the slip case. This is obviously due to the lower velocity gradient at the surface. Results are shown upto $\bar{V} \simeq 2$ where the flow is molecular in nature and the present theory does not hold good. At $\bar{V} \simeq 0.4$ the present theory deviates considerably from the experimental data of Vidal and Bartz [20]. Theoretical results of Shorenstein and Probstein [22], Rudman and Rubin [19] and Suresh Menon [26] are slightly higher than those obtained in the present work even for $\bar{V} < 0.4$ as shown in fig. 6. Fig. 7 shows the effect of semi-wedge angle on skin-friction coefficient. The skin-friction coefficient increases with increase in wedge angle for the obvious reason of larger velocity gradient at the wall. The no-slip solutions give constant values of $M_\infty^3 C_f/2\bar{x}^{3/2}$ for $\bar{V}$ around 0.10. For the slip case on the other hand, the quantity $M_\infty^3 C_f/2\bar{x}^{3/2}$ decreases markedly towards the leading edge.

Variation of the quantity $M_\infty^3 \, St/\bar{x}^{3/2}$ as a function of $\bar{V}$ for various values of $\bar{H}_w$ is shown in fig. 8. Stanton number is observed to be increasing with increase in wall enthalpy ratios. The present results compare quite favourably with the experimental data of Vidal and Bartz [20]. For $\bar{V}$ above 0.4, a comparison with the results of Rudman and Rubin [19] is also given and there is good agreement. Although the theoretical predictions of Shorenstein and Probstein [22] do not agree with the present work above $\bar{V} = 0.4$, they show a reasonable agreement with present theory in the downstream limit. Menon [26] also gives similar results for the merged layer and downstream regimes. In fig. 9, curves (1), (2) and (3) show the effect of wedge angle on the variation of the quantity $M_\infty^3 \, St/\bar{x}^{3/2}$ as a function of the rarefaction parameter. The Stanton number increases with increase in the wedge-angle, which is also indicative of the increased heat transfer. The curve of $M_\infty^3 \, St/\bar{x}^{3/2}$ for $M_\infty = 20$ falls below that for $M_\infty = 10$ for the same values of $\bar{H}_w$, Pr and $\beta$. A comparison between curves (1) and (7) shows that for constant values of $\bar{H}_w$, $M_\infty$ and $\beta$, the Stanton number decreases with increase in Prandtl number.

The variation of slip velocity with rarefaction parameter on a flat plate for different wall enthalpy ratios is shown in fig. 10. Results are shown up to $\bar{V} \simeq 3$ although these extreme regions fall beyond the scope of the continuum analysis. Slip is shown to be clearly dependent on wall temperature, tending

to zero at the extreme cold wall case. Towards the leading edge, the slip velocity becomes a considerable fraction of the free stream velocity. The present results compare reasonably well with the experimental findings of Vidal and Bartz [20] and the theoretical predictions of Shorenstein [22] and Menon [26] upto $\bar{V} \simeq 0.3$ and thereafter shows a comparatively slow rate of increase. Fig. 11 shows the effect of semi-wedge angle and Mach number on slip velocity. Slip is seen to decrease with increase in wedge angle at constant wall cooling. A comparison between curves (1) and (4) clearly shows the dependence of slip velocity on Mach number. The slip velocity over an insulated flat plate is also shown in the same figure and an excellent comparison is noted with the integral analysis of Kumar and Jain [24]. It is interesting to note that the analysis shows the effect of slip even for $\bar{V}$ as low as 0.01, which is a region well within the scope of the strong interaction theory. This figure also gives a first order estimation of $(c. \frac{\lambda_w}{\delta})$ which is approximately equal to $\frac{u_b}{u_\infty}$. For the strong interaction regime, this quantity is much less than unity. Therefore the approximation (2.17a) is justifiable.

Fig. 12 shows the variation of enthalpy jump as a function of rarefaction parameter for different thermal conditions on a flat plate. It can be seen that the enthalpy jump increases as the gas becomes more rarefied. Also a heated surface indicates an increased enthalpy jump in comparison to a cooled surface due to the greater thickness of the Knudsen layer at the plate surface in the former case. In the range $0.055 \leq \bar{V}$ 0.4034, the results obtained in this work show reasonable agreement with the experimental data of Vidal and

Bartz [20]. Theoretical investigations of Shorenstein and Probstein [22] and Menon [26], however, show a slightly lower enthalpy jump.

Fig. 13 shows the temperature jump as a function of $\bar{x}$ for different levels of wall cooling. Towards the leading edge, cooling the wall up to $\bar{H}_w = 0.6$ gives negative temperature jump. Further downstream, the gas rapidly adjusts to the wall temperature. For wall conditions like $\bar{H}_w = 0.2$ and $\bar{H}_w = 0.4$ the temperature jump is positive even close to the leading edge. Thus the temperature jump can be positive or negative depending upon the wall enthalpy variation. This phenomenon was studied in detail by Metcalf [30].

The enthalpy profiles at various plate locations for a semi-cooled wedge are shown in fig. 14. It is seen that the profile becomes fuller as the leading edge is progressively approached. Fig. 15 shows the effect of wall cooling and semi-wedge angle on the distribution of enthalpy across the boundary layer at $\bar{x} = 0.5$. Curves (1), (2) and (3) indicate that the enthalpy profiles become fuller as the wall is heated. Fig. 16 gives the velocity variation across the boundary layer. It is seen that the velocity at the wall decreases with the decrease in wall temperature and strong interaction parameter, and is virtually zero for the fully cooled surface.

## CONCLUSION

*In light of the detailed comparative studies carried out with the experimental as well as theoretical investigations, it is seen that the approximate integral method is quite powerful to handle the hypersonic viscous-inviscid interaction problem with a reasonably good accuracy. The method is relatively simple to use and requires a lesser computational time compared with other techniques. The formulation is so generalised that it includes all the possible flow situations and the solutions appear as a function of Mach number, Reynolds number, Prandtl number, Knudsen number, wall temperature and semiwedge angle.*

*Analysis shows that slip exists even in the strong interaction region and tends asymptotically to about 90% of the free stream velocity towards the leading edge region. The rarefaction effects are reduced with increase in wedge angle and wall-cooling. For the fully cooled surface, slip is apparently absent. The slip solutions give lower values of surface pressure, skin friction, boundary layer thickness, heat transfer etc., compared to no slip solutions. Another noticeable observation is that the temperature jump at the surface can be positive or negative depending upon the value of wall enthalpy ratio.*

*Thus we can say that the slip and temperature jump boundary conditions at the surface are important to explain the experimentally observed plateaus of constant pressure, skin friction, heat transfer etc. and in obtaining results closer to the experimental observations.*

# BIBLIOGRAPHY


(1) Shen, S.F., "An Estimate Viscosity Influences on the Hypersonic Flow over an Insulated Wedge". Journal of Mathematics and Physics, Vol. 31, 1952, pp.192-205.

(2) Shen, S.F., "On Boundary Layer Equations in Hypersonic Flow". Journal of Aeronautical Sciences, Vol. 19, No. 7, July 1952, pp. 500.

(3) Lees, L., "On the Boundary Layer Equations in Hypersonic Flow and its Approximate Solutions". Journal of Aerospaces Sciences, Vol. 20, No. 2, Feb. 1953, pp.143-145.

(4) Stewartson, K., "On the Motion of a Flat Plate at High Speeds in a Viscous Compressible Fluid II". Journal of Aeronautical Sciences, Vol. 22, No. 5, 1955, pp.303-309.

(5) Pai, S.I. and S.F. Shen, "Hypersonic Viscous Flow over a Wedge". 4th Mid Western Conference on Fluid Mechanics". Purdue University 1955, pp. 259-272.

(6) Li, T.Y. and H.T. Nagamatsu, "Hypersonic Viscous Flow on Non-insulated Flat Plate". 4th Mid Western Conference on Fluid Mechanics, Purdue University, 1955, pp. 273.

(7) Bertram, M.H., "Boundary Layer Displacement Effects in Air at Mach Numbers of 6.8 and 9.6", NACA Technical Notes 4133, 1957-1958.

(8) Kendall, J.M., "An Experimental Investigation of Leading Edge Shockwave Boundary Layer Interaction at Mach, 5.9", Journal of Aerospace Sciences, Vol. 24, No. 1, Jan. 1957, pp. 47-57.

(9) Schaaf, S.A., F.C. Hurlbut, L. Talbot and J. Aroesty, "Viscous Interaction at Low Reynolds Numbers". ARS Journal, Vol. 29, 1959, pp. 527-529.

(10) Lees, L., "Influence of Leading Edge Shock Wave on Laminar Boundary Layers at Hypersonic Speeds". Journal of Aeronautic Sciences, Vol. 23, No. 6, June 1956, pp. 596-600.

(11) Nagamatsu, H.T. and Sheer, R.E. Jr., "Hypersonic Shock Wave Boundary Layer Interaction with Leading Edge Slip". ARS Journal, Vol. 31, 1960, pp. 454-462.

(12) Nagamatsu, H.T, Sheer, R.E.,Jr., and J.R. Schmid, "High Temperature Rarefied Hypersonic Flow over a Flat-Plate". ARS Journal, 1961, pp. 902-910.

(13) Cheng, H.K., J. Gordonhall, T.C. Golian and A.Hertzberg, "Boundary Layer Displacement and Leading Edge Bluntness Effects in High Temperature Hypersonic Flow", Journal of Aerospace Sciences, Vol. 29, 1961, pp. 353-381.

(14) Oguchi, H., "Leading Edge Slip Effects in Rarefied Hypersonic Flow". Rarefied Gasdynamics, Suppl. 2, 1963, Vol. II, p. 181.

(15) Edgar Bendore, "Rarefied Viscous Flow Near a Sharp Leading Edge". AIAA Journal, Vol. 1, No. 4, April 1963, pp. 956-959.

(16) Talbot, L., " Criterion for Slip Near Leading Edge of a Flat Plate in Hypersonic Flow". AIAA Journal, Vol. 1, No. 5, May 1963, pp. 1169-1191.

(17) Laurmann, J.A., ''Structure of Boundary Layer at the Leading Edge of a Flat Plate in Hypersonic Slip Flow''. AIAA. Journal, Vol. 2, No. 9, Sept. 1964, pp. 1655-1657.

(18) Aroesty, J., ''Slip Flow and Hypersonic Boundary Layers''. AIAA. Journal, Vol. 2, No. 1, 1964, pp. 149.

(19) Rudman, S. and Rubin, S.G., ''Hypersonic Viscous Flow over Slender Bodies with Sharp Leading Edge''. AIAA Journal, Vol. 6, No. 10, Oct. 1968, pp. 1883-1890.

(20) Vidal, R.J. and Bartz, J.A., ''Surface Measurements on Sharp Flat Plates and Wedges in Low Density Hypersonic Flow''. AIAA. Journal, Vol. 7, No. 6, June, 1969.

(21) Vidal, R.J. and Bartz, J.A. ''An Experimental Study of Hypersonic Low Density Viscous Effects''. AIAA Journal, Preprint No. 63-435, 1963.

(22) Shorenstein, N.L. and Probstein, R.F., ''The Hypersonic Leading Edge Problems'' AIAA Journal, Vol. 6, No. 10, Oct. 1969, pp. 1885-1901.

(23) Maslen, S.H., ''On Heat Transfer in Slip Flow'' Journal of Aerospaces Sciences Vol. 25, No. 6, June 1958, pp.400-401.

(24) Kumar, A. and Jain, A.C., ''Hypersonic Viscous Slip Flow over Insulated Wedges''. AIAA Journal, Vol. 10, No. 8, August 1972, pp. 1081-1083.

(25) Partho Chaudhury, ''Hypersonic Rarefied Viscous-Inviscid Interaction on Insulated Wedges''. M.Tech. Thesis, Department of Aeronautical Engg., I.I.T. Kanpur, May 1978.

(26) Suresh Menon, ''An Analysis of Strong Interaction Problem with Slip and Temperature-Jump Effects''. M. Tech. Thesis, Department of Aeronautical Engg. Indian Institute of Technology Kanpur, July 1978.

(27) Chattopadhyay, ''Unsteady Flows at High Mach Numbers over Slender Wedge Wings''. Ph.D. Thesis, University of Alberta Edmonton, 1972.

(28) Vidal, K.J. and Wittliff, C.E., ''Hypersonic Low Density Studies of Blunt and Slender Bodies''. Rarefied Gas-dynamics, Vol. II, Suppl. 2, 1963, pp. 343-378.

(29) Vas, I.E., J. Mcdougall, G. Koppen-Wallner, and S.M. Bogdonoff, ''Some Exploratory Experimental Studies of Hypersonic Low Density Effects on Flat Plates and Cones''. Rarefied Gasdynamics , Suppl. No. 3, Vol. 1, 1965, pp. 509.

(30) Metcalf, S.C., Lillicrap, D.C., and Berry, C.J., '' A Study of the Effect of the Surface - Temperature on Shock Layer Development over Sharp Edged Shapes in Low Reynolds Number High Speed Flow''. Rarefied Gasdynamics , Suppl. No. 5, Vol. 1, 1969, pp. 619.

(31) Kennard, E.H., ''Kinetic Theory of Gases''. McGraw-Hill, New York, 1938, Indian ed. 1962.

(32) Nagamatsu, H.T., ''Summary of Recent 'GALCIT' Hypersonic Experimental Investigations''. Journal of Aeronautical Sciences, Vol. 22, No. 3, March 1955, pp. 165.

(33) Hammit, A.G., Bogdonoff, S.M., ''A Study of the Flow about Simple Bodies at Mach Numbers from 11 to 15'' Princeton University Aeronautical Engineering Laboratory Report No. 277, Sept. 1954.

(34) Oguchi, H., ''The Sharp Leading Edge Problems in Hypersonic Flow''. Rarefied Gasdynamics , Suppl. 1, 1961, pp. 501-524.

(35) Hayes, W.D. and R.F. Probstein, ''Hypersonic Flow Theory''. Academic Press, New York and London 1959.

(36) McGroskey, W.J., Bogdonoff, S.M. and McDougall J.G., ''An Experimental Model for the Sharp Plate in Rarefied Hypersonic Flow''. AIAA. Journal, Vol. 24, No. 9, 1966, pp. 1580-1587.

(37) Becker, M. and Boylan, D.E., ''Experimental Flow Field Investigations Near the Sharp Leading Edge of a Cooled Flat Plate in Hypersonic Low Density Flow''. Rarefied Gas Dynamics, Suppl. 4, Vol. 2, 1967, pp. 993-1015.

(38) Pan, Y.S. and Probstein, R.F., ''Rarefied Flow Transition at Leading Edge''. Fundamental Phenomena in Hypersonic Flow (J.G. Hall Ed.) Cornell University Press, Ithaca, 1966, pp. 259-306.

(39) Chow, W.L., ''Hypersonic Rarefied Flow Past the Sharp Leading Edge of a Flat Plate'' AIAA Journal, Vol. 5, No. 9, Sept., 1967, pp. 1549-1556.

(40) Chow, W.L., ''Hypersonic Slip Flow Past the Leading Edge of a Flat Plate''. AIAA Journal, Vol. 4, 1966, pp. 2062-2063.

(41) Vas, I.E. and Allegre, ''The N-4, Hypersonic Low Density Facility and Some Preliminary Results on a Sharp Flat Plate'' Rarefied Gasdynamics, Suppl. 4, Vol. II, 1967, pp.1015-1031.

(42) McCroskey, W.J., Bogdonoff, S.M. and A.P. Genchi, ''Leading Edge Flow Studies of Sharp Bodies in Rarefied Hypersonic Flow''. Rarefied Gasdynamics , Suppl. 4, Vol. II, 1967, pp. 1047-1066.

(43) Joss, W.W., Vas, I.E., Bogdonoff, S.M., ''Studies of Leading Edge Effects on the Rarefied Hypersonic Flow over a Flat Plate''. AIAA-Journal, Vol. 5, 1968.

(44) Charwat, A.F., ''Molecular Flow Study of Hypersonic Sharp Leading Edge Interaction'', Rarefied gas Dynamics Suppl.,1, 1961, pp. 551-578.

(45) Chattopadhyay and Rodkiewicz, C.M., ''Hypersonic Strong Interaction Flow over an Inclined Surface '' AIAA Journal Vol. 9, No. 3, March 1971, pp. 535-537.

(46) Kogan, M.N., ''Rarefied Gasdynamics'' Plenum Press, New York, 1969.

(47) Martino, R.L., ''Heat Transfer in Slip Flow'' University of Toronto, UTIA Report No. 35, October 1955.

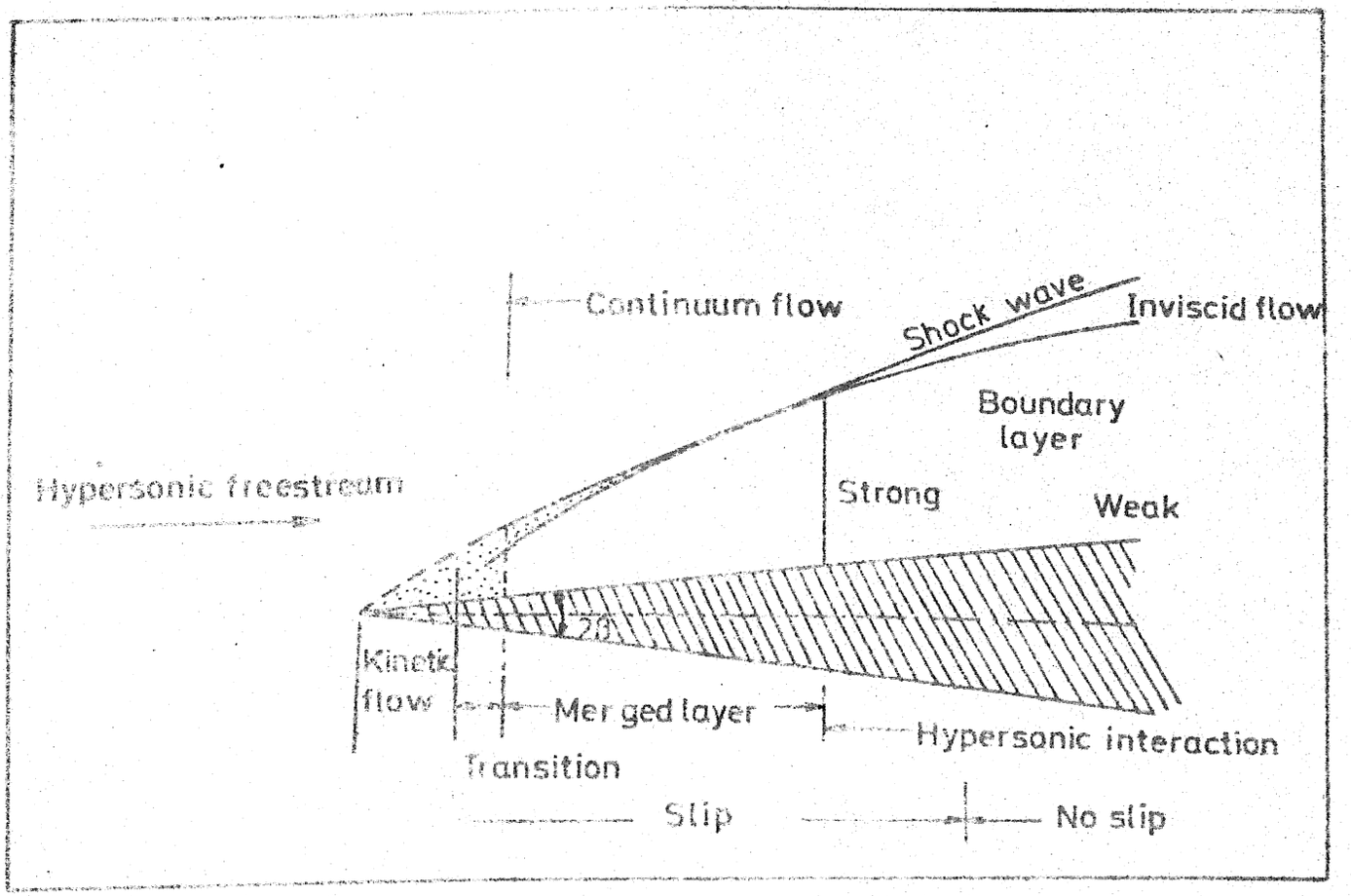


Fig.1 Flow regimes of the hypersonic rarefied flow past a sharp nosed slender body

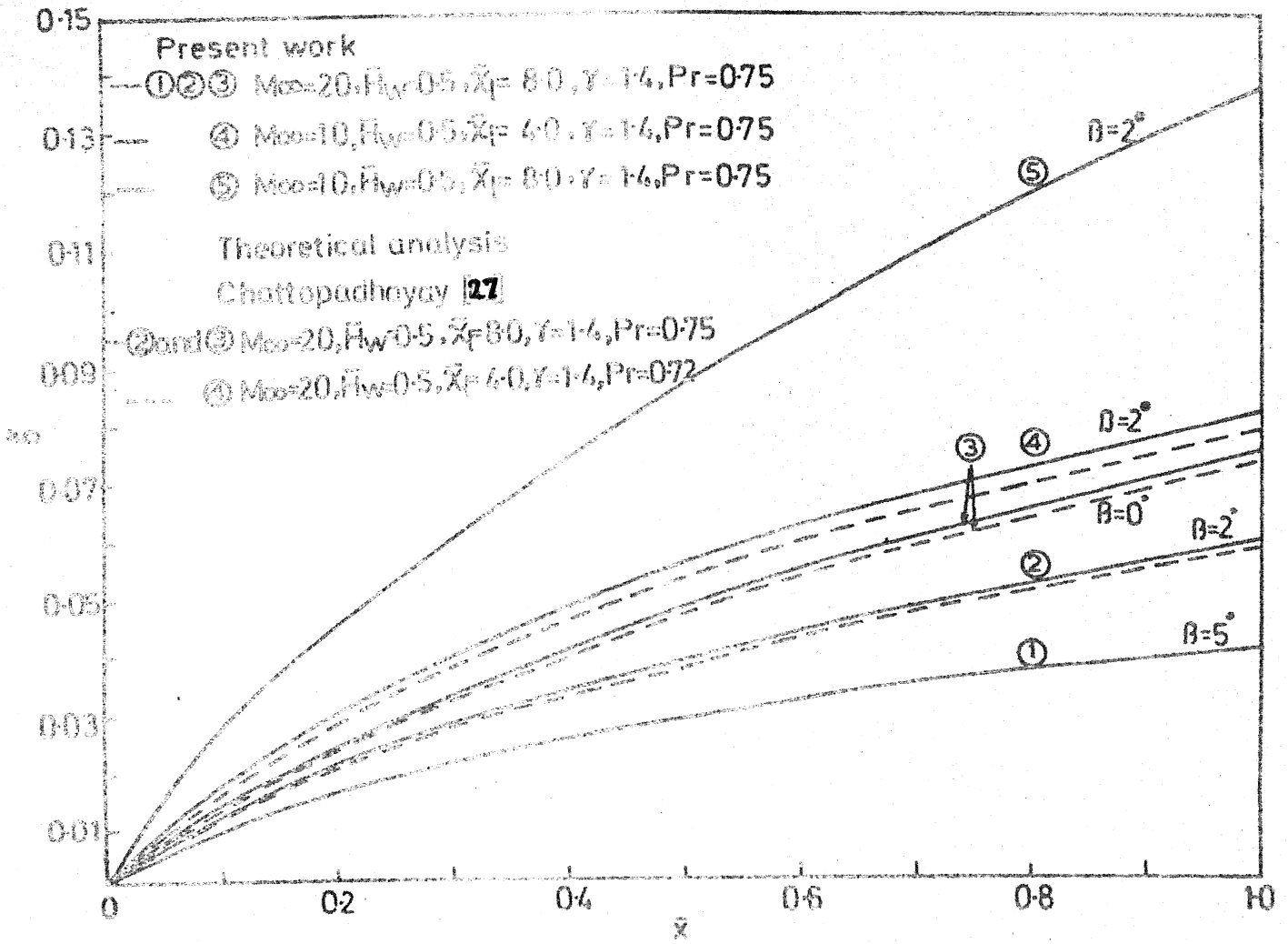


Fig.2 Effect of semiwedge angle and Mach number on boundary layer thickness distribution over a cold wall

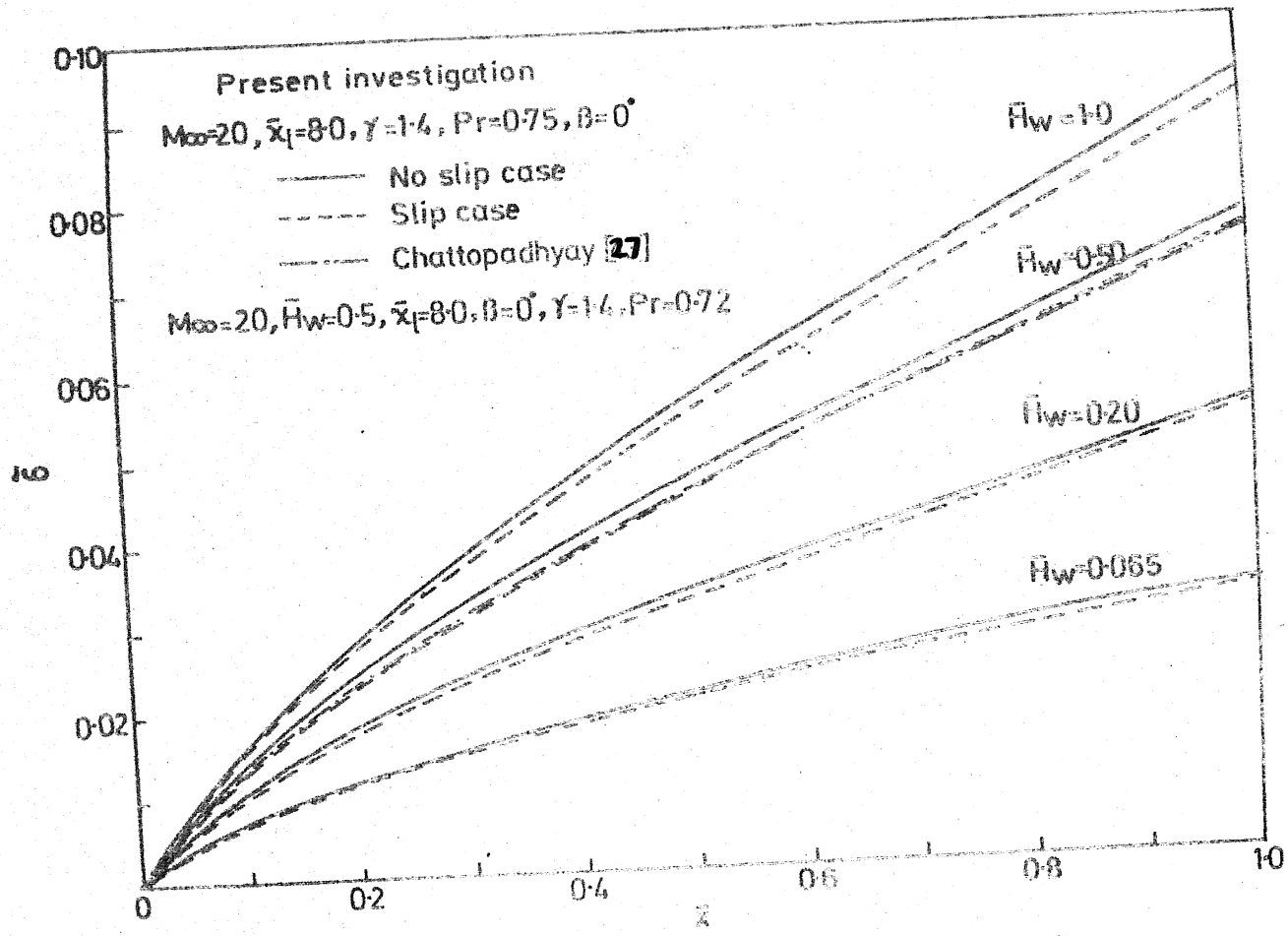


Fig.3 Effect of wall enthalpy ratio on boundary layer thickness distribution over a flat plate

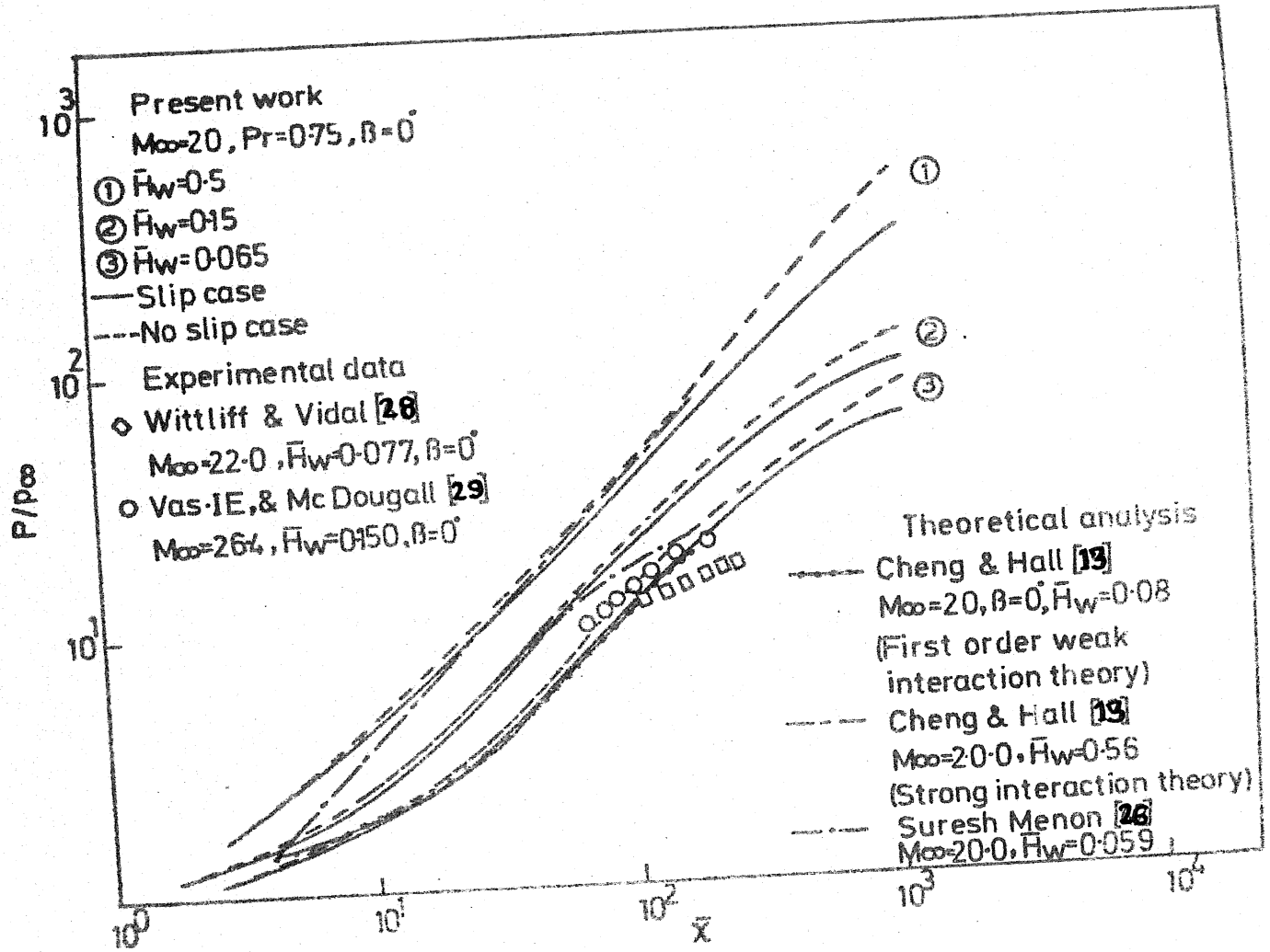


Fig.4 Pressure distribution as a function of strong interaction parameter

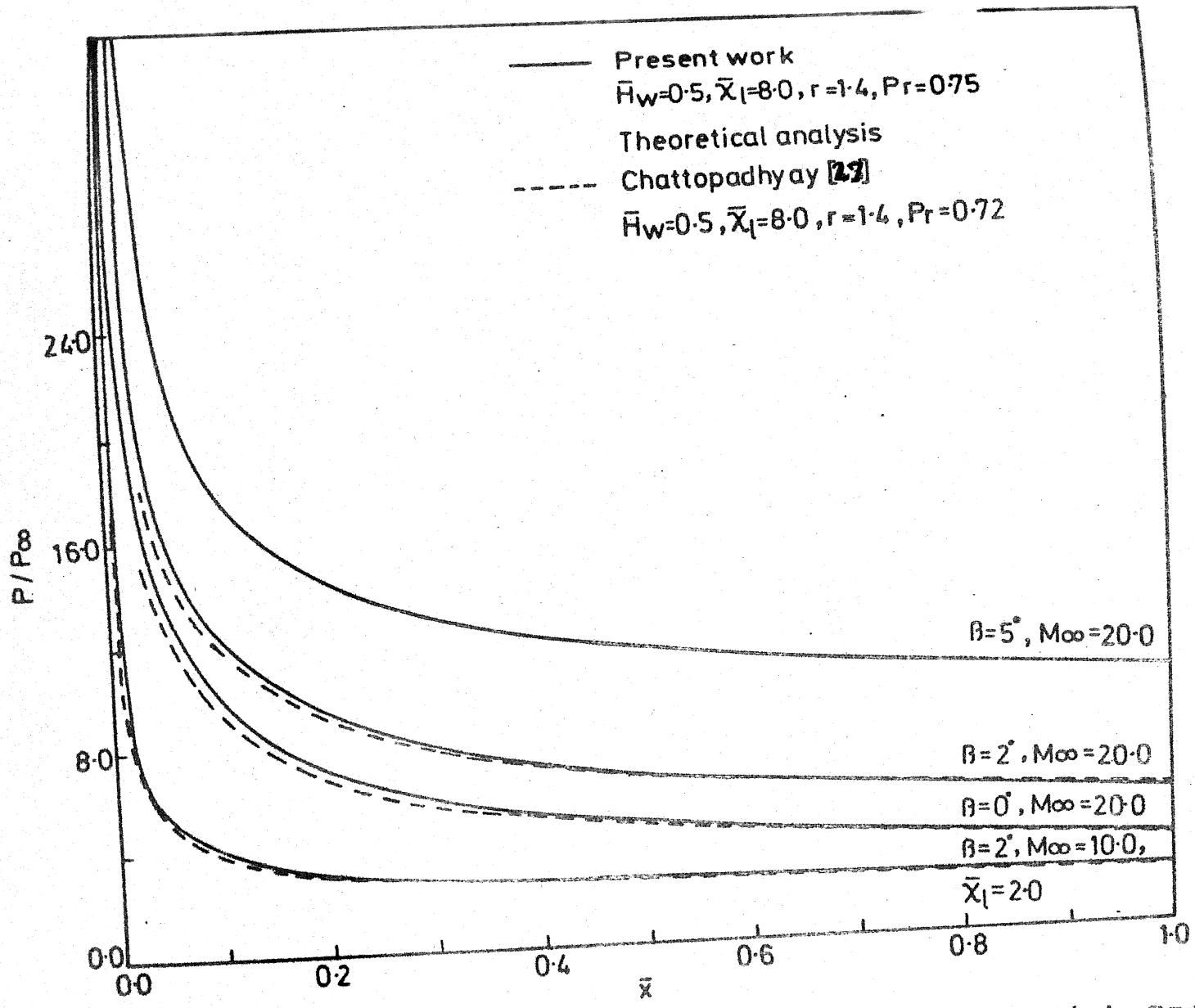


Fig.5 Comparison of pressure distribution over a flat plate and wedge (cold wall case)

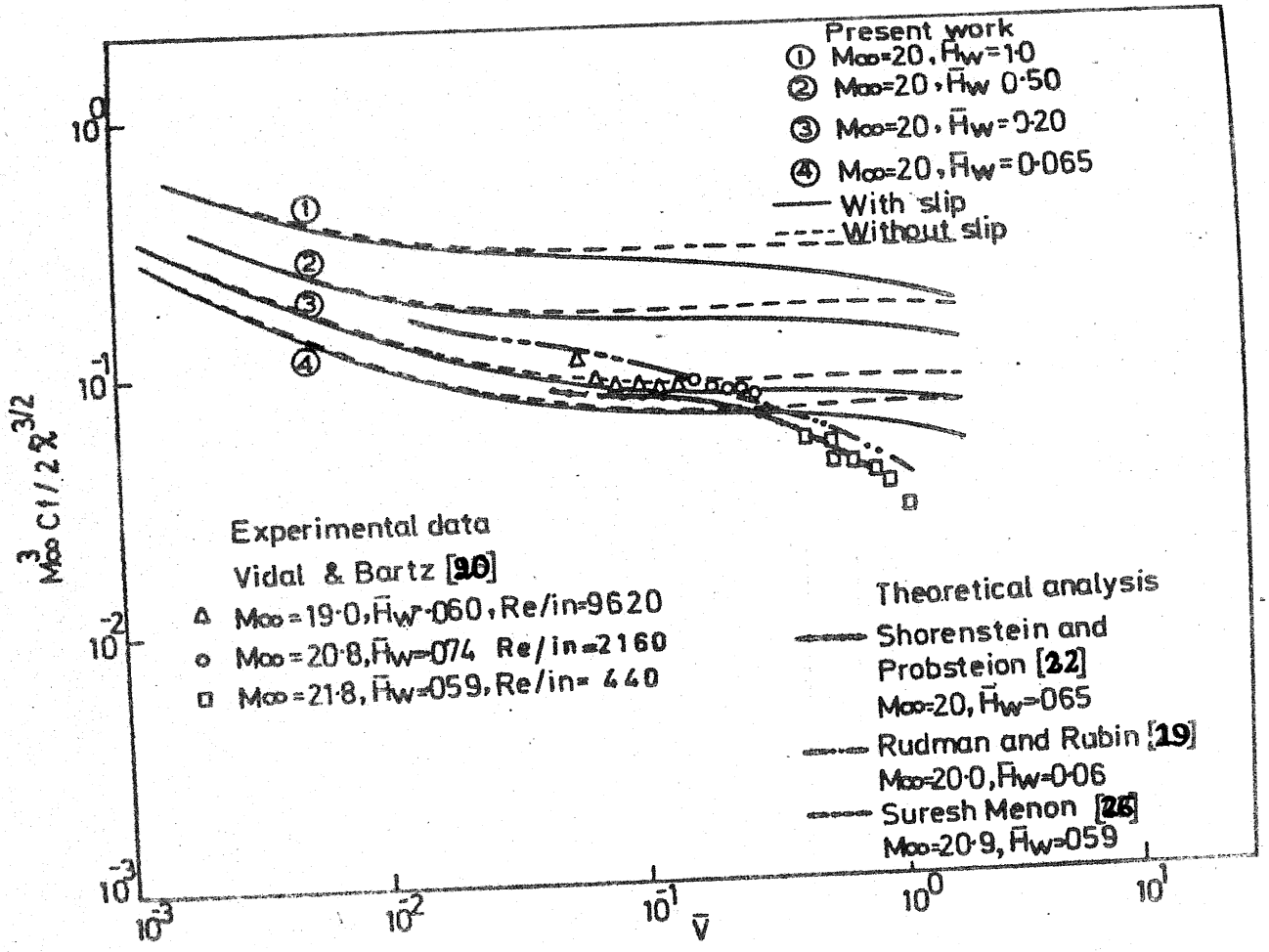


Fig.6 Variation of skinfriction as a function of rarefaction parameter (Effect of wall enthalpy ratio on skin friction)

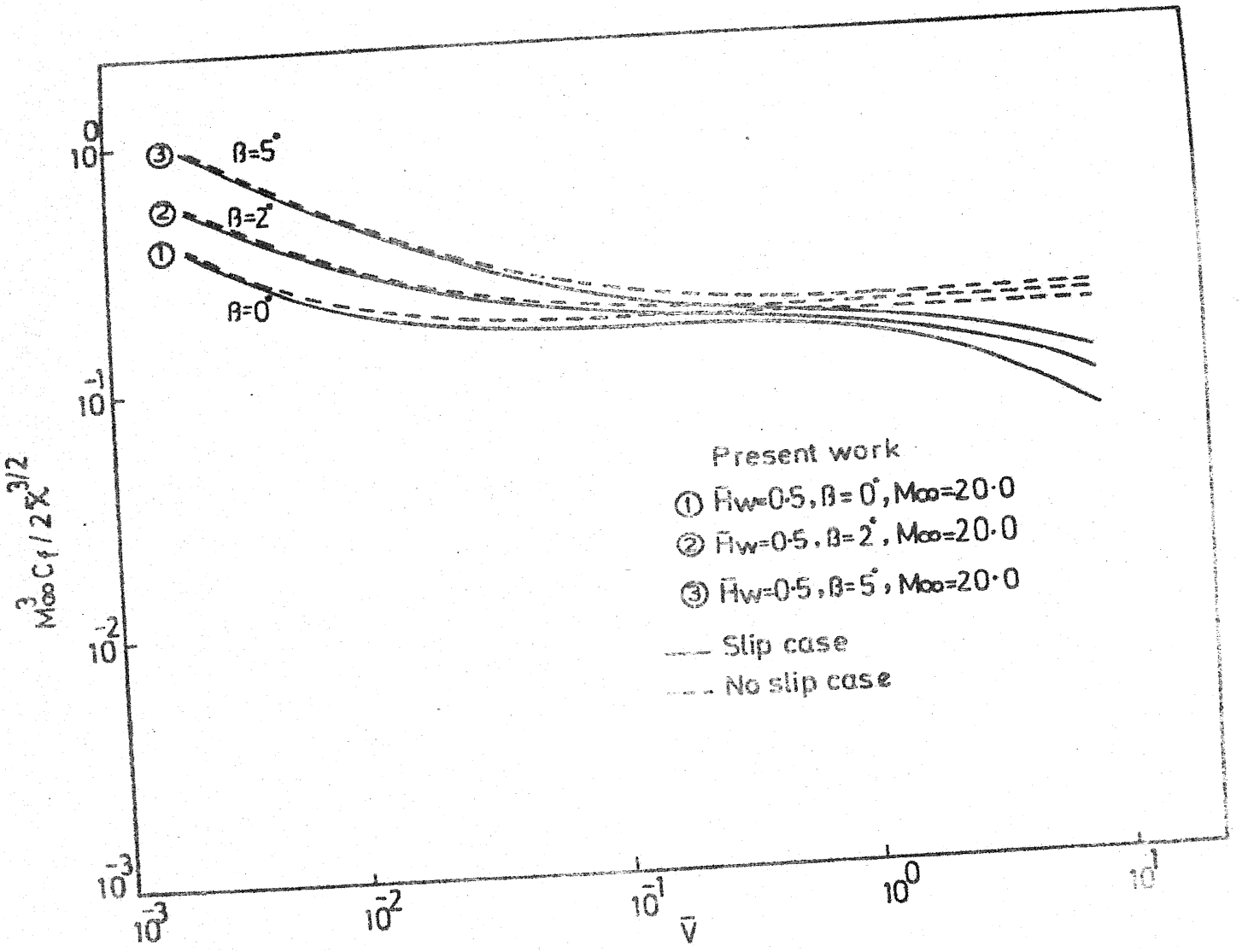


Fig.7 Variation of skin friction with rarefaction parameter
(Effect of semi-wedge angle on skin friction)

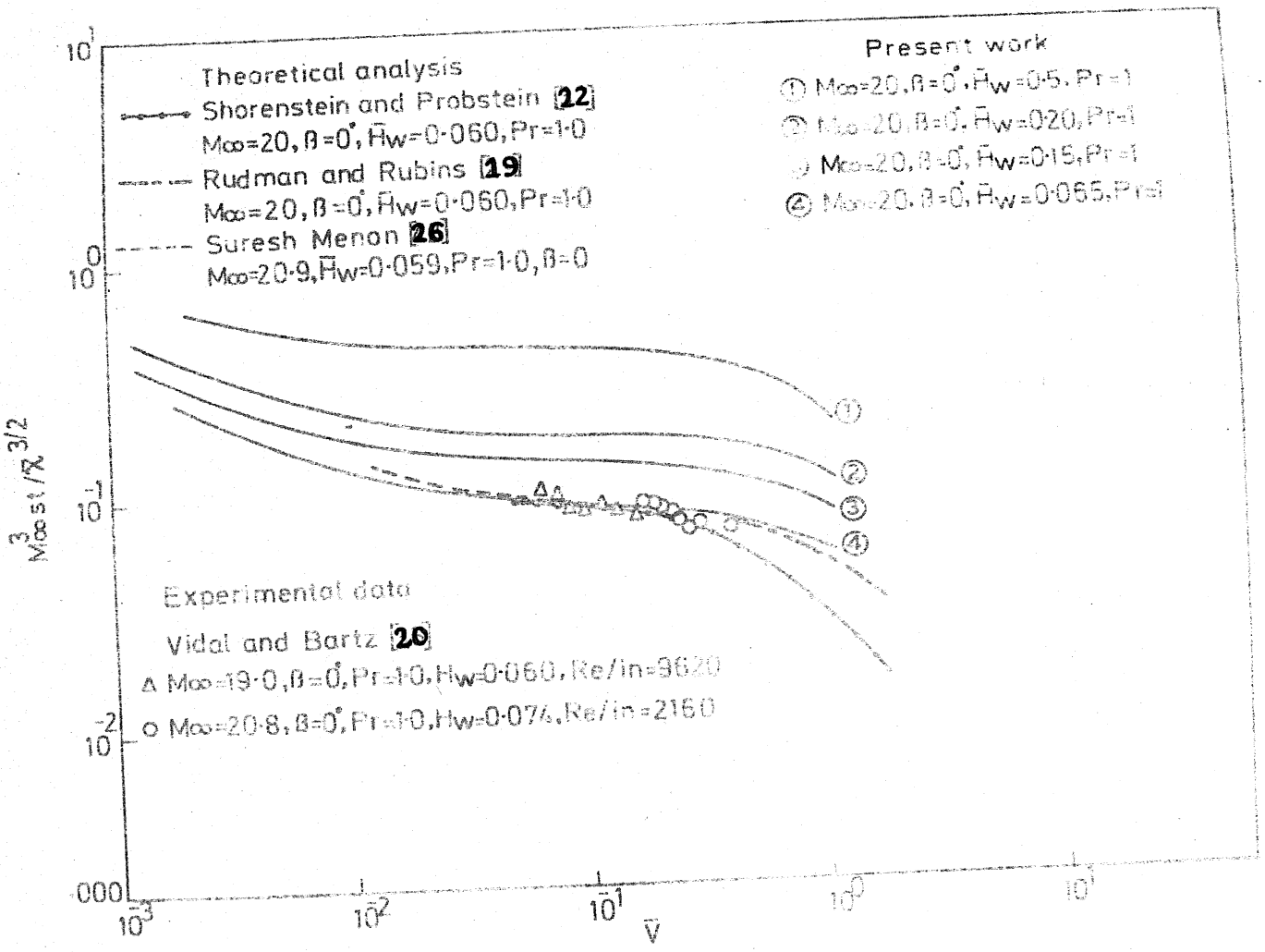


Fig.8 Variation of stanton number as a function of rarefaction parameter
(Effect of wall enthalpy ratios on stanton number)

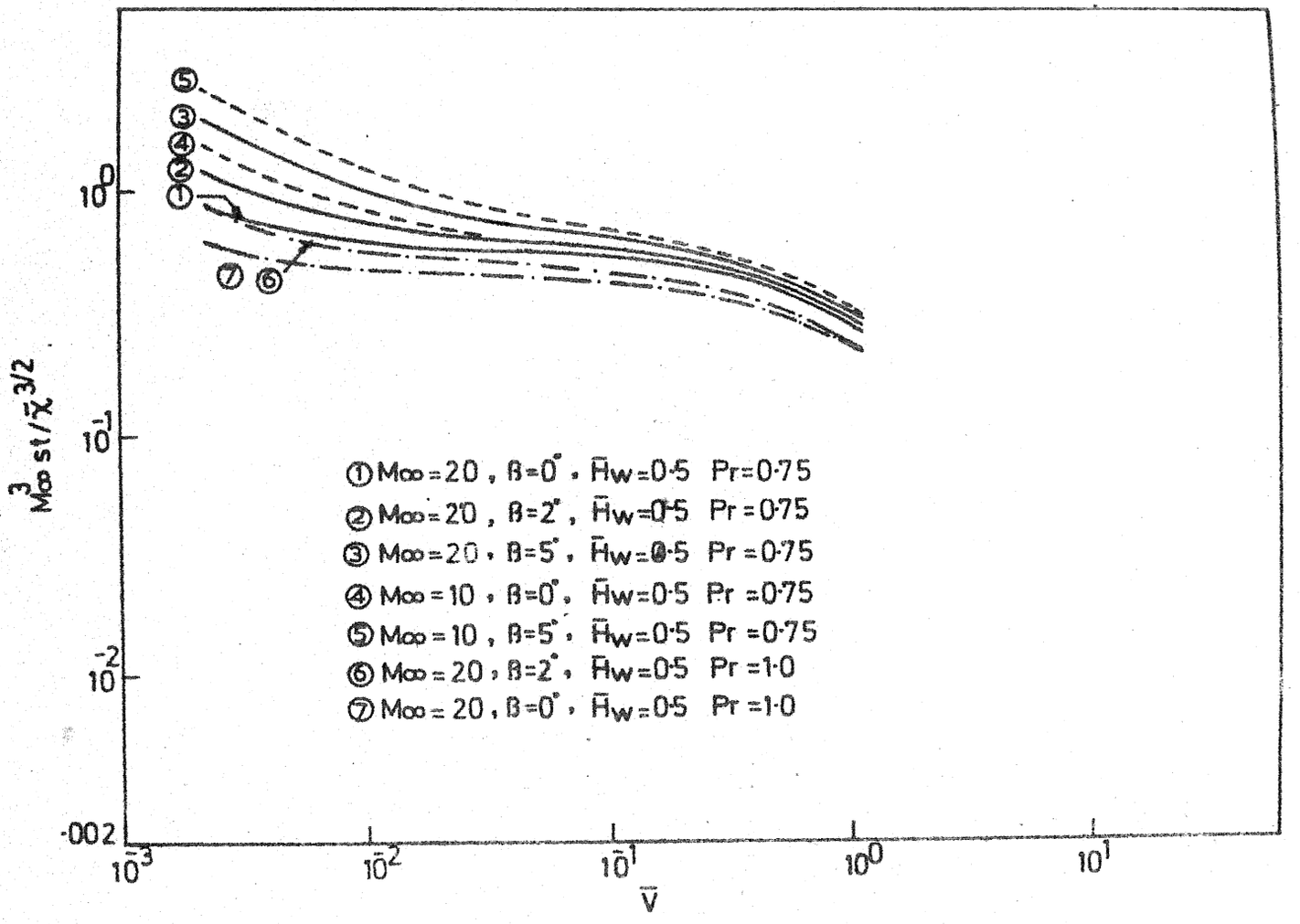


Fig. 9 Variation of stanton number with rarefaction parameter
(Effect of semi-wedge angle, Mach number & prandtl number on stanton number)

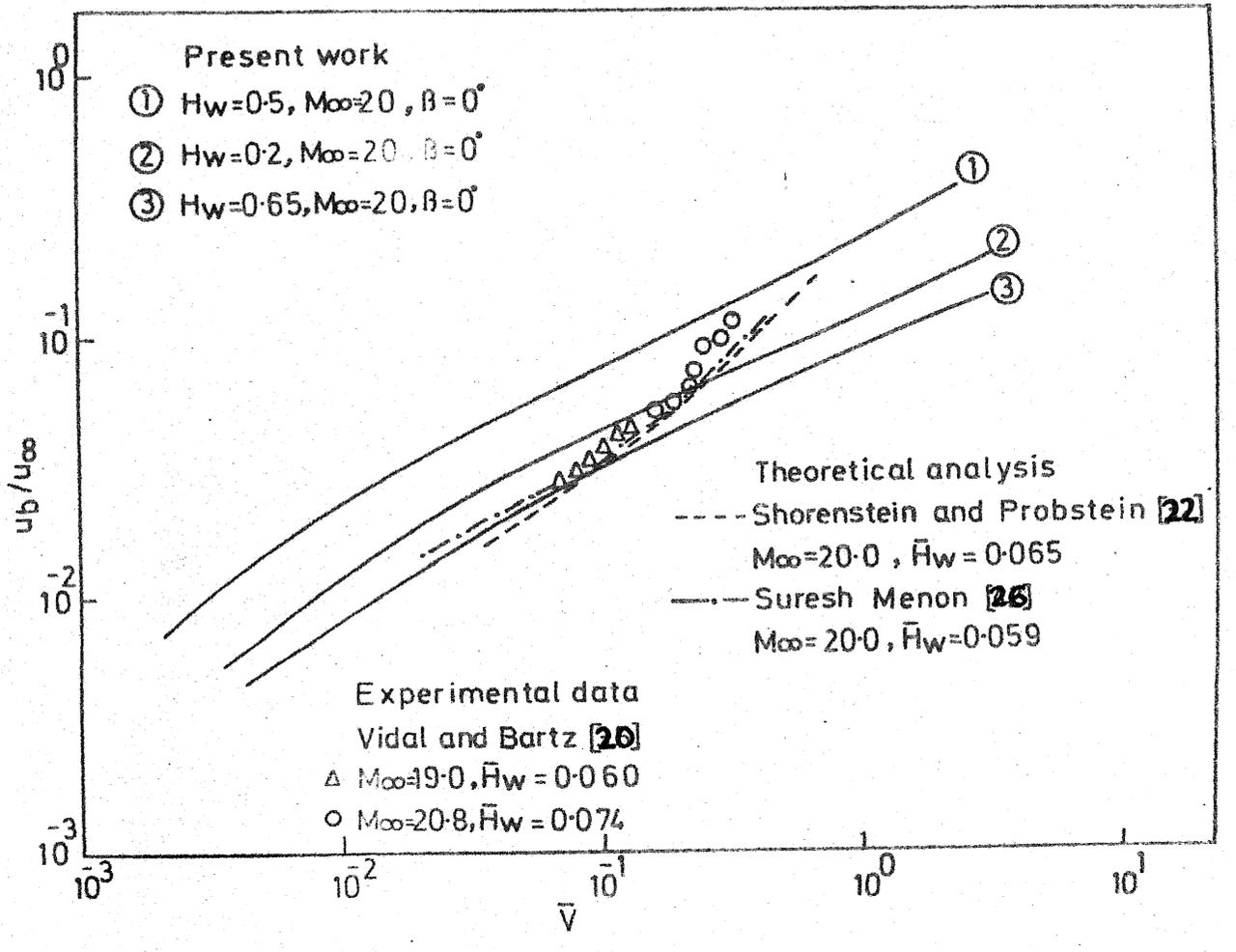


Fig.10 Variation of slip velocity with rarefaction parameter (Effect of wall enthalpy ratio on slip velocity).

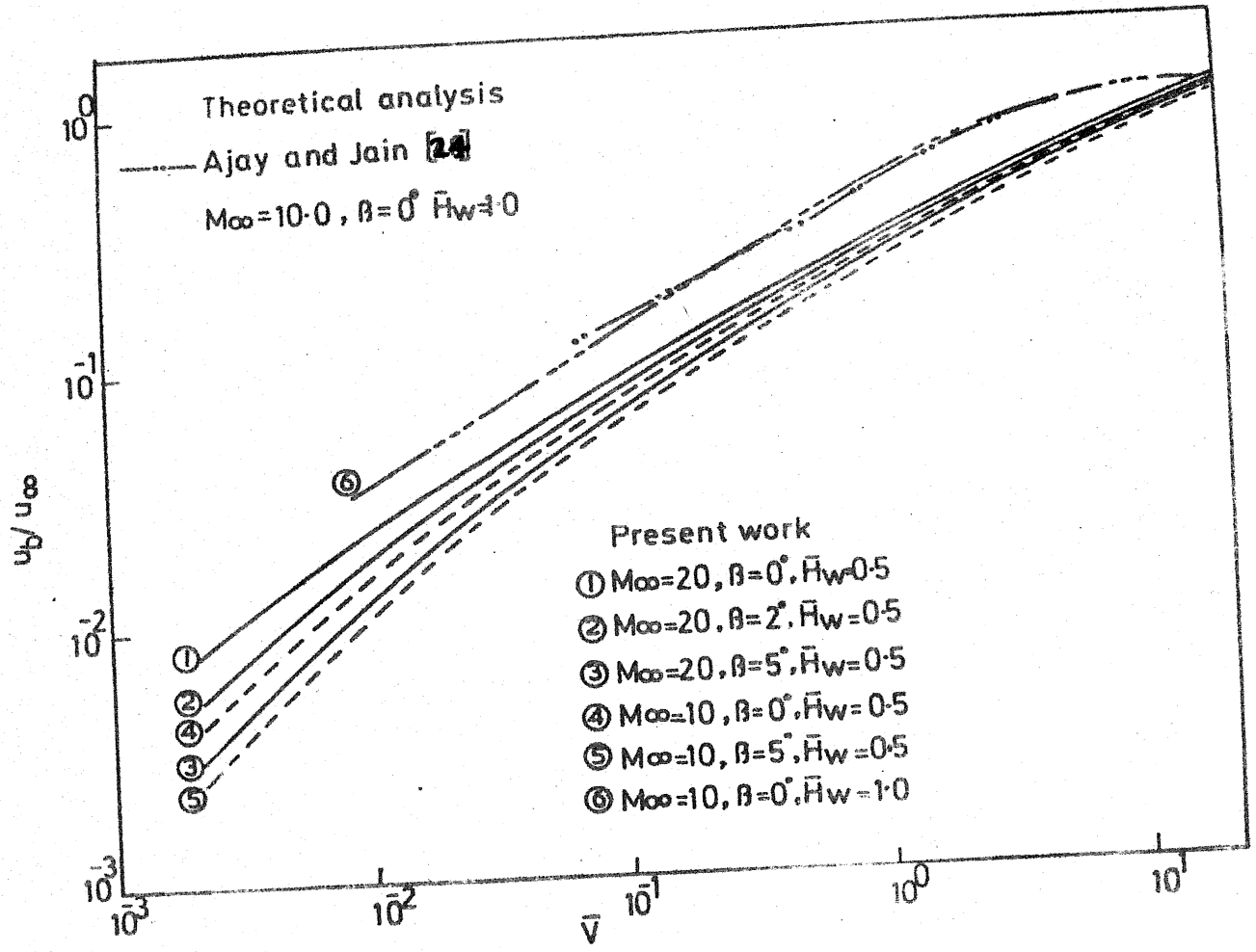


Fig.11 Variation of slip velocity as a function of rarefaction parameter (Effect of semi-wedge angle and Mach number on slip velocity)

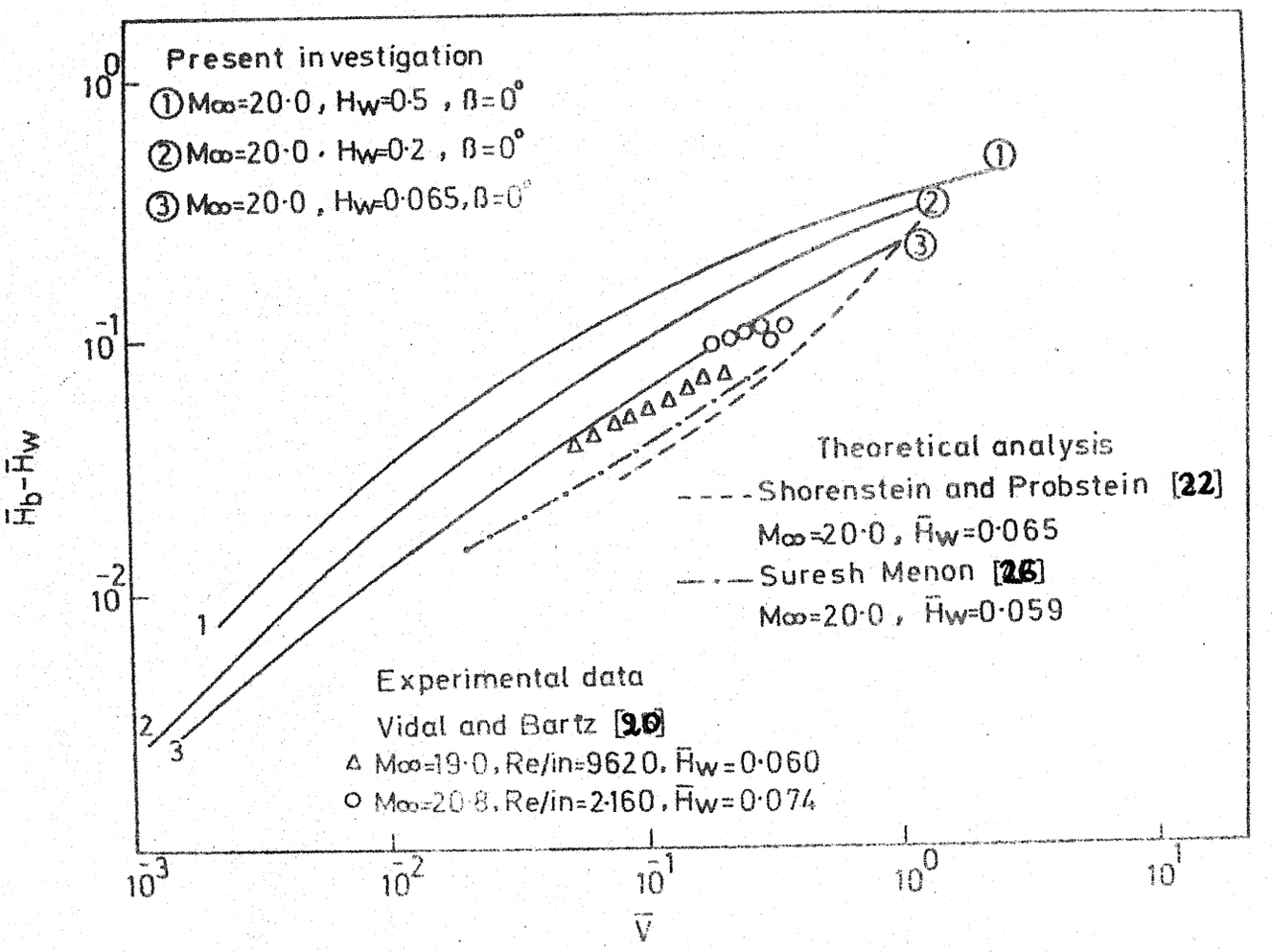


Fig.12 Variation of enthalpy jump with rarefaction parameter

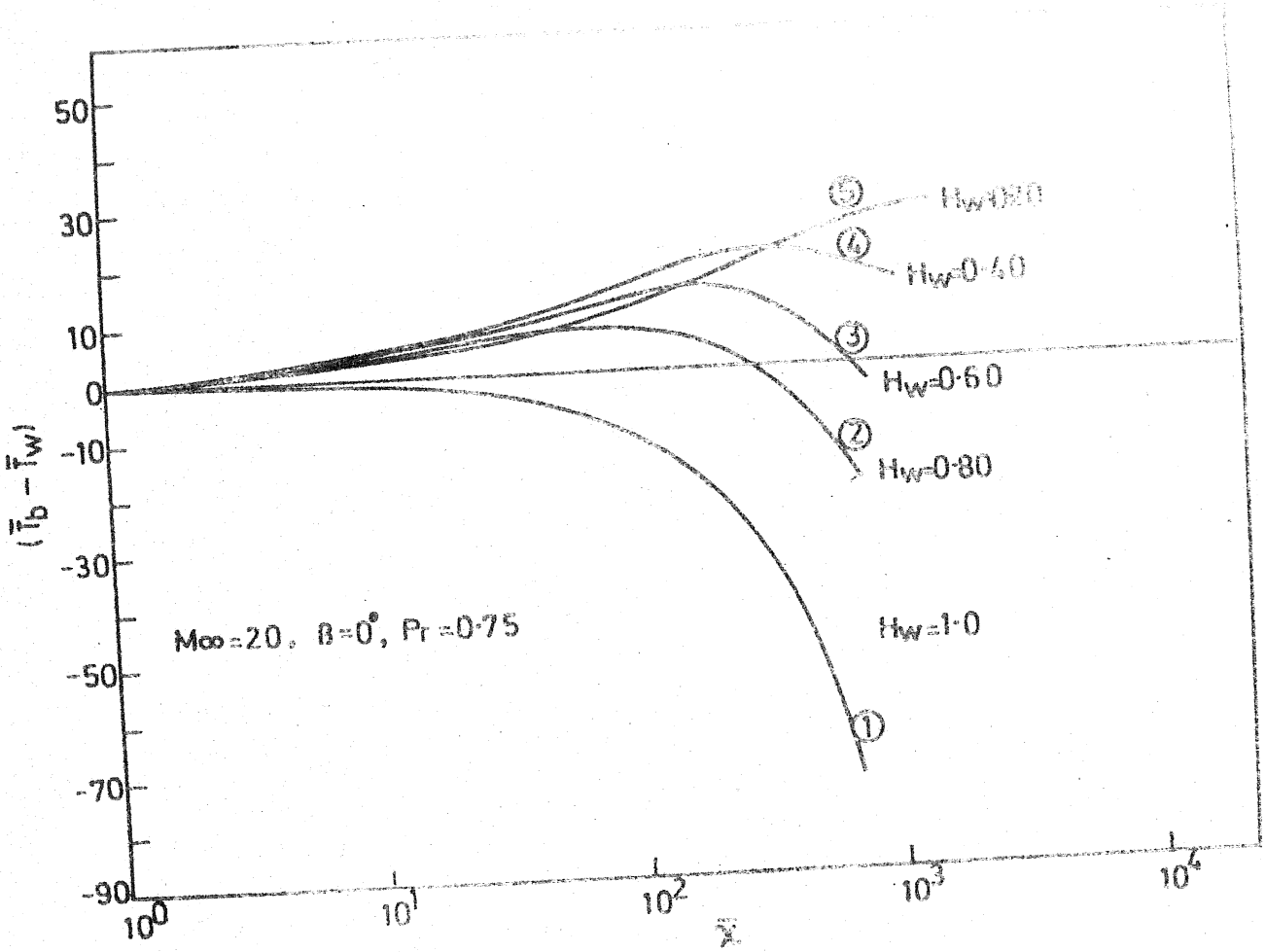


**Fig. 13** Variation of temperature jump as a function of strong interaction parameter

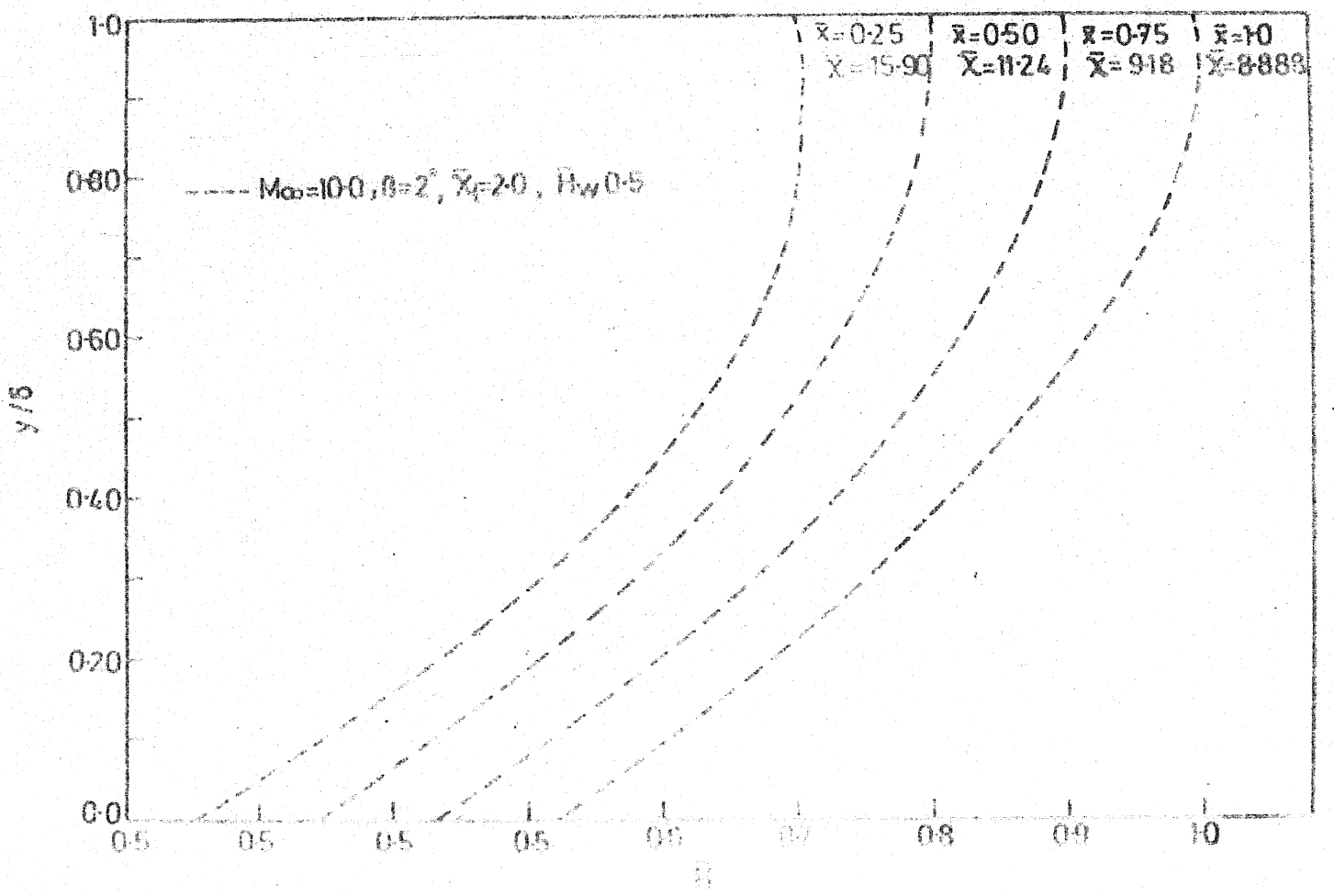


Fig.14 Variation of the enthalpy profiles with distance along the wedge (Effect of blockage on enthalpy profiles)

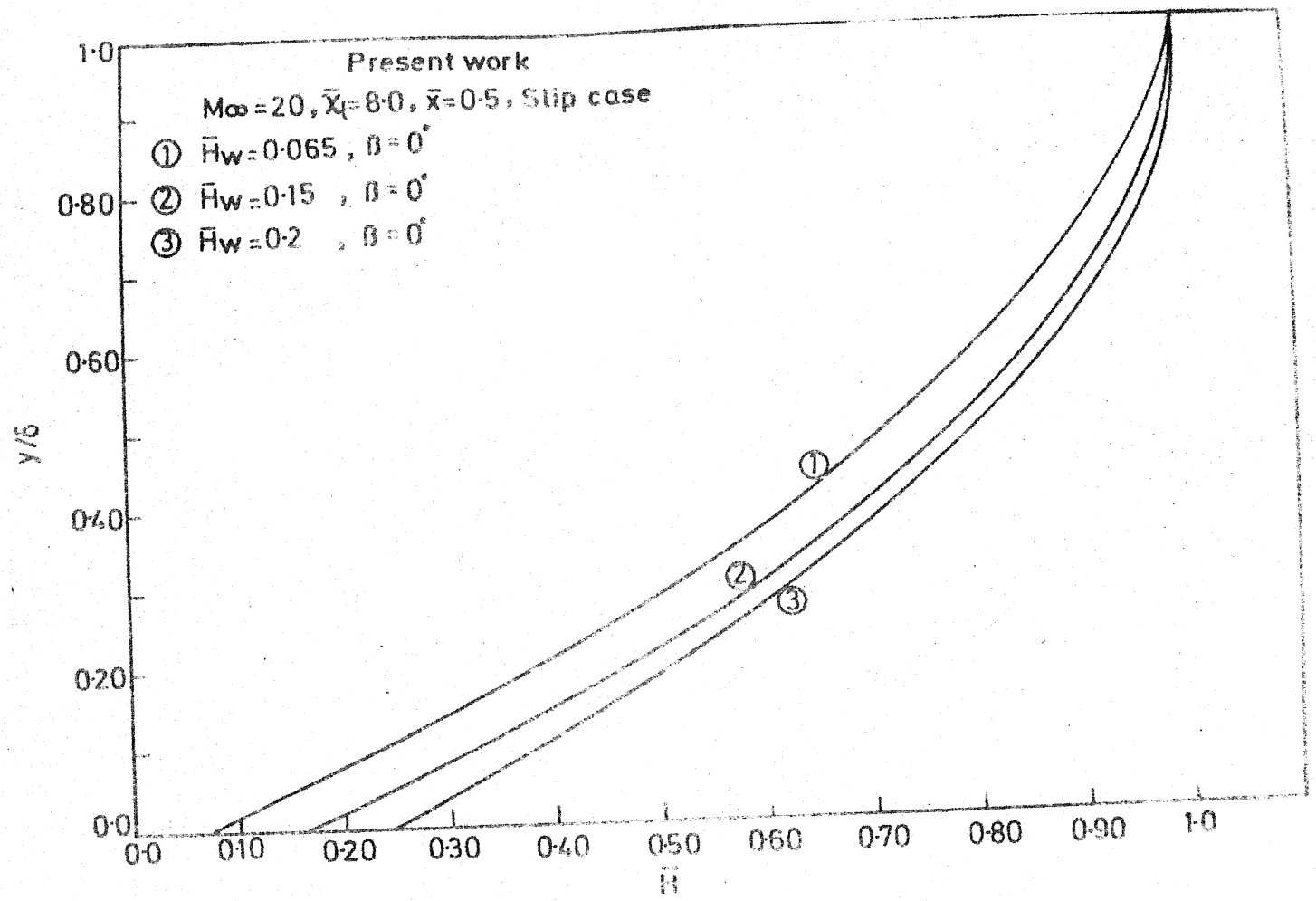


Fig.15 Variation of enthalpy across the boundary layer (Effect of wall enthalpy ratio and semi wedge angle on enthalpy distribution)

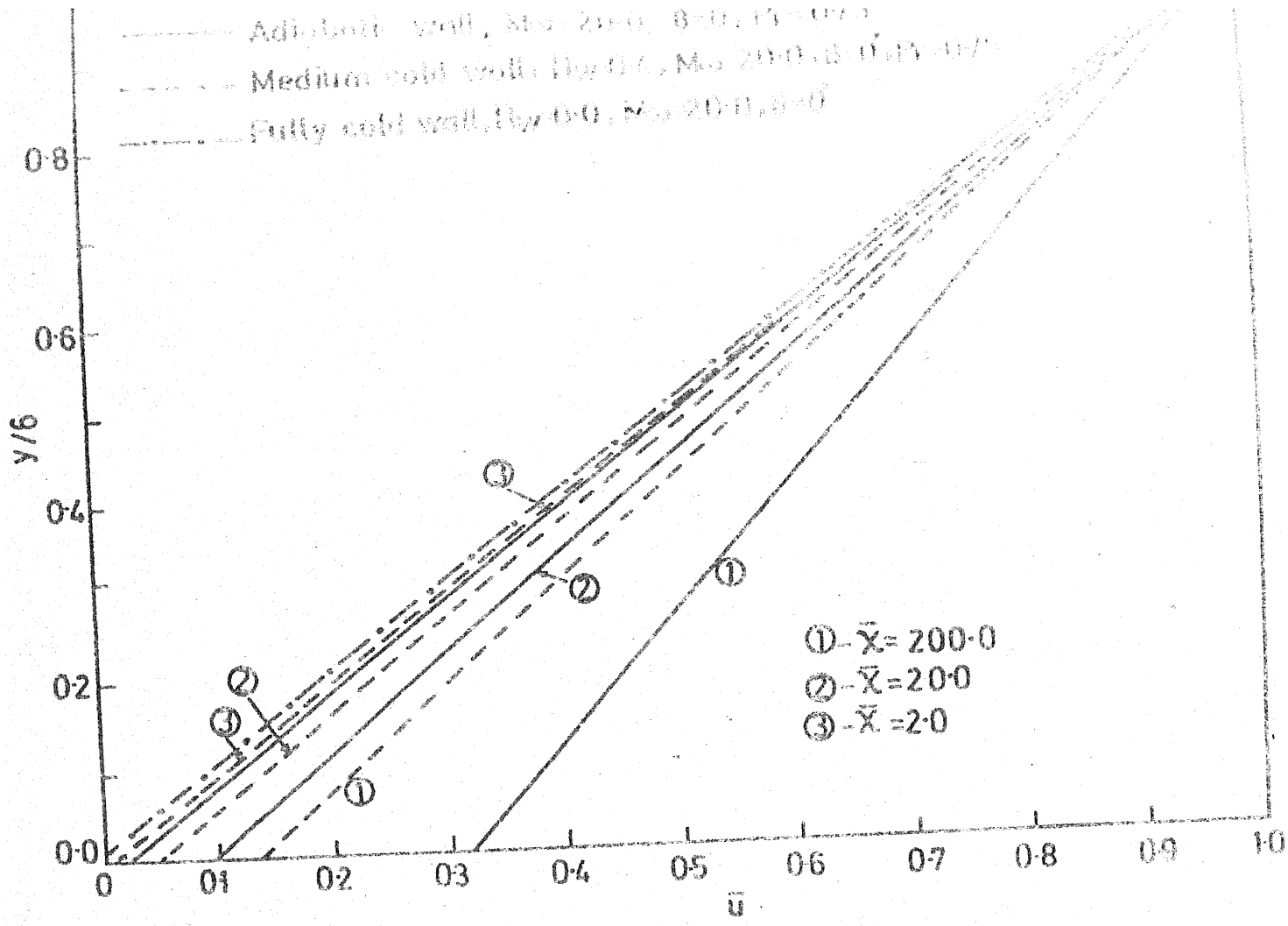


Fig.16 Velocity profiles at various stations along the surface (Adiabatic wall, medium cold wall and extremely cold wall)

## APPENDIX

### § A-1 THE SLIP PARAMETERS

From the kinetic theory (31) we may write :

$$\lambda_w = 1.256\ \gamma^{1/2}\ \mu_w / a_w\ \rho_w$$

or

$$\frac{\lambda_w}{L} = 1.256\ \gamma^{1/2}\ \frac{\rho_\infty\ u_\infty}{a_w\ \rho_w}$$

$$= 1.256\ \gamma^{1/2}\ \frac{u_\infty}{a_\infty}\ \frac{a_\infty}{a_w}\ \frac{\rho_\infty}{\rho_w}$$

$$= 1.256\ \gamma^{1/2}\ M_\infty \sqrt{\frac{T_\infty}{T_w}} \times \frac{\rho_\infty}{\rho_w}$$

i.e. $$\frac{\lambda_w}{L} = \frac{1.256\ \sqrt{\gamma}\ M_\infty\ \sqrt{T_w/T_\infty}}{P/P_\infty} \ . \qquad (A-1)$$

Further,

$$\frac{T_w}{T_\infty} = \frac{H_w}{H_\infty - \frac{1}{2}\ u_\infty^2}$$

$$= \bar{H}_w\ (1 + \frac{\gamma-1}{2}\ M_\infty^2).$$

For hypersonic flows with $M_\infty^2 >> 1$, one can write

$$\frac{T_w}{T_\infty} \simeq \bar{H}_w\ (\frac{\gamma-1}{2})\ M_\infty^2 \qquad (A-2)$$

Substituting (A-2) in (A-1) gives

$$\frac{\lambda_w}{L} = \frac{1.256\, M_\infty^2 \sqrt{\frac{\gamma(\gamma-1)}{2}\ \bar{H}_w}}{(P/P_\infty)} \,. \qquad \text{(A-3)}$$

When pressure is described by a tangent-wedge approximation valid for strong-interaction region only as given by(2.22), one obtains from (A-3) :

$$\frac{\lambda_w}{L} = \frac{1.256}{\gamma+1} \sqrt{\frac{2(\gamma-1)\ \bar{H}_w}{\gamma}}\ \frac{1}{\left(\beta + \frac{d\delta}{dx}\right)^2} \,. \qquad \text{(A-4)}$$

Equations (A-4) enables us to define the two slip parameters as

$$\left.\begin{aligned} e_{11} &= \frac{C_1\, \lambda_w}{L}\,(\beta + \eta')^2 = \frac{1.256}{\gamma+1}\, C_1 \left[2\,\frac{(\gamma-1)}{\gamma}\,\bar{H}_w\right]^{1/2} \\ \text{and} \\ e_{22} &= \frac{C_2\, \lambda_w}{L}\,(\beta + \eta')^2 = \frac{1.256}{\gamma+1}\, C_2 \left[2\,\frac{(\gamma-1)}{\gamma}\,\bar{H}_w\right]^{1/2} \end{aligned}\right\} \qquad \text{(A-5)}$$

We also define two other slip parameters from (A-3), such that it doesn't impose any restriction on how the pressure is being described :

$$\left.\begin{aligned} e_1 &= \frac{C_1\, \lambda_w}{L}\,\frac{1}{\omega} = 1.256\, C_1 \left[\gamma\,\frac{(\gamma-1)}{2}\ \bar{H}_w\right]^{1/2} \\ e_2 &= \frac{C_2\, \lambda_w}{L}\,\frac{1}{\omega} = 1.256\, C_2 \left[\gamma\ \frac{(\gamma-1)}{2}\ \bar{H}_w\right]^{1/2} \end{aligned}\right\} \qquad \text{(A-6)}$$

wherein (A-6)

$$\omega = M_\infty^2/(P/P_\infty).$$

## §A.2. VELOCITY AND ENTHALPY PROFILES

For computational purposes the velocity and enthalpy profiles given by (2.12) and (2.16) respectively are non-dimensionalised using the characteristic length 'L' as given below:

Equation (2.12) gives

$$\frac{u}{u_\infty} = \frac{C_1 \lambda_w + y}{C_1 \lambda_w + \delta}$$

$$= \frac{\frac{C_1 \lambda_w}{L} + y/L}{\frac{C_1 \lambda_w}{L} + \frac{\delta}{L}}$$

or $$\frac{u}{u_\infty} = \frac{e_1 \omega + \phi}{e_1 \omega + \eta} \qquad (A-7)$$

wherein (A-7), $\phi = y/L$.

Similarly the expression (2.16) gives the non-dimensionalised enthalpy profile as

$$\bar{H}_w = (\bar{H}_w + e_2 \omega\psi) + \psi\phi + \left[ (1-\bar{H}_w) - \psi(e_2 \omega + \eta) \right] \phi^2/\eta^2 \qquad (A-8)$$

wherein (A-7) and (A-8), $\phi$ varies from zero to $\eta$.

The slip velocity, $u_b$ is computed form (A-7) with $\phi = 0$ :

$$\frac{u_b}{u_\infty} = \frac{e_1 \omega}{e_1 \omega + \eta} \qquad (A-9)$$

## § A.3. SKIN FRICTION COEFFICIENT

By definition the shear stress at the wall is

$$\tau_w = \mu_w \left(\frac{\partial u}{\partial y}\right)_w .$$

Substitution for $\left(\frac{\partial u}{\partial y}\right)_w$ from (2.12) leads to

$$\tau_w = \frac{\mu_w \, u_\infty}{C_1 \, \lambda_w + \delta} .$$

Now, the skin friction coefficient may be defined as

$$C_f = \frac{\tau_w}{\frac{1}{2} \rho_\infty u_\infty^2}$$

i.e., $$C_f = 2 \frac{\mu_w}{\rho_\infty u_\infty} \frac{1}{(C_1 \lambda_w + \delta)} = \frac{2L}{C_1 \lambda_w + \delta}$$

or $$C_f = \frac{2}{e_1 \omega + \eta} . \qquad (A\text{-}10)$$

## § A.4. STRONG INTERACTION PARAMATER

The strong-interaction parameter is defined as

$$\bar{\chi} = M_\infty^3 \sqrt{\frac{c}{Re_x}} .$$

Further, using the linear temperature-viscosity law

$$\frac{\mu_w}{\mu_\infty} = c \frac{T_w}{T_\infty} \quad \text{in the following definition of } \xi :$$

$$\xi = \frac{x}{L} = \frac{\rho_\infty u_\infty x}{\mu_w} = \frac{\rho_\infty u_\infty x}{\mu_\infty} \frac{\mu_\infty}{\mu_w} .$$

We obtain,

$$\xi = \frac{Re_x}{c\,\frac{T_w}{T_\infty}} = \frac{Re_x}{\bar{H}_w\,(1 + \frac{\gamma-1}{2} M_\infty^2)\,c}$$

or
$$\xi = \frac{M_\infty^6}{(M_\infty^3 \sqrt{c/Re_x})^2\, \bar{H}_w(1 + \frac{\gamma-1}{2} M_\infty^2)}$$

$$= \frac{M_\infty^6}{\bar{H}_w\,(1 + \frac{\gamma-1}{2} M_\infty^2)\,\bar{x}^2} \quad .$$

This may be rearranged to give :

$$\bar{x} = \frac{M_\infty^3}{\sqrt{\bar{H}_w\,(1 + \frac{\gamma-1}{2} M_\infty^2)\,\xi}} \quad . \qquad \text{(A-11)}$$

## §A.5. HEAT TRANSFER AND STANTON NUMBER

By definition, the heat transfer at the body surface is given by

$$\dot{q}_w = (-k\,\frac{\partial T}{\partial y})_w \quad .$$

Also, from the definition of H :

$$(\frac{\partial T}{\partial y})_w = \frac{1}{C_p}\,(\frac{\partial H}{\partial y})_w - \frac{1}{2}\,(\frac{\partial u^2}{\partial y})_w \quad .$$

Evaluating $(\frac{\partial u^2}{\partial y})_w$ and $(\frac{\partial H}{\partial y})_w$ from the expressions (2.12) and (2.16) for the velocity and total enthalpy profiles, respectively, we get

$$\dot{q}_w = \left(-\frac{k\, H_\infty}{C_p}\right)_w \left[ B - \frac{2C_1 \lambda_w}{(C_1 \lambda_w + \delta)^2} \right]$$

$$\text{or } \dot{q}_w = \left(\frac{-k}{C_p}\right)_w H_\infty \left[ \frac{\psi}{L} - \frac{1}{L} \frac{\frac{2\, C_1 \lambda_w}{L}}{\frac{(C_1 \lambda_w + \delta)^2}{L}} \right]$$

$$\text{or } \dot{q}_w = \left(\frac{-k}{\mu\, C_p}\right)_w \rho_\infty\, u_\infty\, H_\infty \left[ \psi - \frac{2e_1 \omega}{(e_1 \omega + \eta)^2} \right] \qquad \text{(A-12)}$$

Stanton number, by definition, is

$$St = - \frac{\dot{q}_w}{\rho_\infty\, u_\infty\, C_p\, (T_o - T_w)}$$

or

$$St = - \frac{\dot{q}_w}{\rho_\infty\, u_\infty\, H_\infty\, (1 - \bar{H}_w)} .$$

Substituting $\dot{q}_w$ from (A-12) gives :

$$St = \frac{1}{P_r\, (1 - \bar{H}_w)} \left[ \psi - \frac{2e_1 \omega}{(e_1 \omega + \eta)^2} \right] . \qquad \text{(A-13)}$$

All these results for no-slip cases can be computed by equating the slip parameters to zero.